

Maximum Volume Inscribed Ellipsoid: A New Simplex-Structured Matrix Factorization Framework via Facet Enumeration and Convex Optimization

Chia-Hsiang Lin[†], Ruiyuan Wu[‡], Wing-Kin Ma[‡], Chong-Yung Chi[†], and Yue Wang^{*}

[†]Institute of Communications Engineering, National Tsing-Hua University, Hsinchu, Taiwan 30013, R.O.C.

Emails: chiahsiang.steven.lin@gmail.com, cychi@ee.nthu.edu.tw

[‡]Department of Electronic Engineering, The Chinese University of Hong Kong, Shatin, New Territories, Hong Kong.

Emails: rywu@ee.cuhk.edu.hk, wkma@ieee.org

^{*}Department of Electrical and Computer Engineering, Virginia Polytechnic Institute and State University, VA, USA.

Email: yuewang@vt.edu

October 25, 2018

Abstract

Consider a structured matrix factorization scenario where one factor is modeled to have columns lying in the unit simplex. Such a simplex-structured matrix factorization (SSMF) problem has spurred much interest in key topics such as hyperspectral unmixing in remote sensing and topic discovery in machine learning. In this paper we develop a new theoretical framework for SSMF. The idea is to study a maximum volume ellipsoid inscribed in the convex hull of the data points, which has not been attempted in prior literature. We show a sufficient condition under which this maximum volume inscribed ellipsoid (MVIE) framework can guarantee exact recovery of the factors. The condition derived is much better than that of separable non-negative matrix factorization (or pure-pixel search) and is comparable to that of another powerful framework called minimum volume enclosing simplex. From the MVIE framework we also develop an algorithm that uses facet enumeration and convex optimization to achieve the aforementioned recovery result. Numerical results are presented to demonstrate the potential of this new theoretical SSMF framework.

Index Terms: maximum volume inscribed ellipsoid, simplex, structured matrix factorization, facet enumeration, convex optimization

1 Introduction

Consider the following problem. Let $\mathbf{X} \in \mathbb{R}^{M \times L}$ be a given data matrix. The data matrix \mathbf{X} adheres to a low-rank model $\mathbf{X} = \mathbf{AS}$, where $\mathbf{A} \in \mathbb{R}^{M \times N}$, $\mathbf{S} \in \mathbb{R}^{N \times L}$ with $N \leq \min\{M, L\}$. The goal is to recover \mathbf{A} and \mathbf{S} from \mathbf{X} , with the aid of some known or hypothesized structures with \mathbf{A} and/or \mathbf{S} . Broadly speaking, such a kind of problems is called *structured matrix factorization (SMF)*. We narrow down our attention to an SMF problem subclass coined *simplex-SMF (SSMF)* in this paper. In SSMF, the matrix factor \mathbf{S} is assumed to have columns lying in the unit simplex. Simple as the assumption seems, SSMF has been found to be elegant and powerful—as suggested

by years of research in a specific topic in geoscience and remote sensing [8, 40] and as shown by more recent research in areas such as computer vision, machine learning, text mining and optimization [29].

In geoscience and remote sensing, SSMF has been extensively considered under the topic of hyperspectral unmixing (HU). It deals with decomposition of a remotely sensed hyperspectral image into endmember spectral signatures and the corresponding abundance maps, and it is one of the main topics in hyperspectral imaging for remote sensing. There, a widely accepted assumption is that \mathbf{S} has columns lying in the unit simplex. Or, some data pre-processing may be applied to make the aforementioned assumption happen [8, 16, 29, 41]. Among the many techniques proposed in HU, we should mention pure-pixel search and minimum volume enclosing simplex (MVES) [9, 14, 20, 36, 37, 42]—they are insightful and are recently shown to be theoretically sound [15, 30, 38].

In machine learning, on the other hand, we have recently seen much interest in using non-negative matrix factorization (NMF) to tackle the problem of topic discovery in text mining. In particular, the separable NMF framework has attracted considerable attention [1, 2, 21, 22, 24, 25, 28, 44] because it allows one to perform SSMF tractably; specifically, via simple algorithms or via convex optimization. Separable NMF also assumes that the columns of \mathbf{S} lie in the unit simplex, and thus it also falls in the SSMF scope. Separable NMF is very closely related to pure-pixel search in HU, but with new twists not seen in traditional HU such as convex optimization-based solutions. Readers are also referred to [33] for a recent work that applies the MVES notion in HU to topic discovery. Other than HU and topic discovery, SSMF and related concepts also find applications in various areas such as gene expression data analysis, dynamic biomedical imaging, and analytical chemistry [17, 39, 45].

From a theoretical viewpoint, pure-pixel search, separable NMF and MVES are beautiful. They elegantly utilize the geometric structures of the SSMF model to pin down sufficient conditions for exact recovery, and then show how such recovery can be accomplished when building an algorithm. We will shed some light onto those geometric insights when we review the problem in the next section, and we should note that recent theoretical breakthroughs in SSMF have played a key role in understanding the fundamental natures of SSMF better and in designing better algorithms. Motivated by such exciting advances, in this paper we explore a new theoretical direction for SSMF. Our idea is still geometrical, but we use a different way, namely, by considering the maximum volume ellipsoid inscribed in a data-constructed convex hull; the intuition will be elucidated later. As the main contribution of this paper, we will show a sufficient condition under which this maximum volume inscribed ellipsoid (MVIE) framework achieves exact recovery. The sufficient recovery condition we prove is arguably not hard to satisfy in practice and is much better than that of pure-pixel search and separable NMF; and coincidentally it is the same as that of MVES. In addition, our development will reveal that MVIE can be practically realized by solving a facet enumeration problem, and then by solving a convex optimization problem in form of log determinant maximization. This shows a very different flavor from the MVES framework in which we are required to solve a non-convex problem. While we should point out that our MVIE solution may not be computed in polynomial time because of the computational difficulty with facet enumeration in the worst-case sense, it still brings a new perspective to the SSMF problem. In particular, for instances where facet enumeration can be efficiently computed, the remaining problem with MVIE is to solve a convex problem in which local minima are no longer an issue. We will provide numerical results to demonstrate the potential of the MVIE framework.

The organization of this paper is as follows. We succinctly review the SSMF model and some

existing frameworks in Section 2. The MVIE framework is described in Section 3. Section 4 provides the proof of the main theoretical result in this paper. Section 5 develops an MVIE algorithm and discusses computational issues. Numerical results are provided in Section 6, and we conclude this work in Section 7.

Our notations are standard, and some of them are specified as follows. Boldface lowercase and capital letters, like \mathbf{a} and \mathbf{A} , represent vectors and matrices, respectively (resp.); unless specified, \mathbf{a}_i denotes the i th column of \mathbf{A} ; \mathbf{e}_i denotes a unit vector with $[\mathbf{e}_i]_i = 1$ and $[\mathbf{e}_i]_j = 0$ for $j \neq i$; $\mathbf{1}$ denotes an all-one vector; $\mathbf{a} \geq \mathbf{0}$ means that \mathbf{a} is element-wise non-negative; the pseudo-inverse of a given matrix \mathbf{A} is denoted by \mathbf{A}^\dagger ; $\|\cdot\|$ denotes the Euclidean norm (for both vectors and matrices); given a set \mathcal{C} in \mathbb{R}^n , $\text{aff } \mathcal{C}$ and $\text{conv } \mathcal{C}$ denote the affine hull and convex hull of \mathcal{C} , resp.; the dimension of a set \mathcal{C} is denoted by $\dim \mathcal{C}$; $\text{int } \mathcal{C}$, $\text{ri } \mathcal{C}$, $\text{bd } \mathcal{C}$ and $\text{rbd } \mathcal{C}$ denote the interior, relative interior, boundary and relative boundary of the given set \mathcal{C} , resp.; $\text{vol } \mathcal{C}$ denotes the volume of a measurable set \mathcal{C} ; $\mathcal{B}_n = \{\mathbf{x} \in \mathbb{R}^n \mid \|\mathbf{x}\| \leq 1\}$ denotes the n -dimensional unit Euclidean-norm ball, or simply unit ball; \mathbb{S}^n and \mathbb{S}_+^n denote the sets of all $n \times n$ symmetric and symmetric positive semidefinite matrices, resp.; $\lambda_{\min}(\mathbf{X})$ and $\lambda_{\max}(\mathbf{X})$ denote the smallest and largest eigenvalues of \mathbf{X} , resp.

2 Data Model and Related Work

As described above, we consider a low-rank data model $\mathbf{X} = \mathbf{AS}$. Let us adopt a column-by-column representation

$$\mathbf{x}_i = \mathbf{As}_i, \quad i = 1, \dots, L,$$

and recall that $\mathbf{A} \in \mathbb{R}^{M \times N}$, $\mathbf{s}_i \in \mathbb{R}^N$ for all i . We assume that

- (A1) every \mathbf{s}_i lies in the unit simplex, i.e., $\mathbf{s}_i \geq \mathbf{0}$, $\mathbf{1}^T \mathbf{s}_i = 1$;
- (A2) \mathbf{A} has full column rank;
- (A3) $\mathbf{S} = [\mathbf{s}_1, \dots, \mathbf{s}_L]$ has full row rank;

and they will be assumed without explicit mentioning in the sequel. The problem is to recover \mathbf{A} and \mathbf{S} from the data points $\mathbf{x}_1, \dots, \mathbf{x}_L$. Since \mathbf{s}_i 's lie in the unit simplex, we call this problem simplex-structured matrix factorization, or SSMF in short. We will focus only on recovery of \mathbf{A} from $\mathbf{x}_1, \dots, \mathbf{x}_L$; \mathbf{S} can be recovered by solving an inverse problem once \mathbf{A} is retrieved.

SSMF finds many important applications as we reviewed in the Introduction. And one can find an enormous amount of literature—from remote sensing, signal processing, machine learning, computer vision, optimization, etc.—on the wide variety of techniques for SSMF or related problems. Here we selectively and concisely describe two mainstream frameworks. One is called pure-pixel search in HU in remote sensing [40] or separable NMF in machine learning [29]. Both assume that for every $k \in \{1, \dots, N\}$, there exists an index $i_k \in \{1, \dots, N\}$ such that

$$\mathbf{s}_{i_k} = \mathbf{e}_k.$$

The above assumption is called the pure-pixel assumption in HU or separability assumption in separable NMF. Figure 1(a) illustrates the geometry of $\mathbf{s}_1, \dots, \mathbf{s}_L$ under the pure-pixel assumption, where we see that the pure pixels $\mathbf{s}_{i_1}, \dots, \mathbf{s}_{i_N}$ are vertices of the convex hull $\text{conv}\{\mathbf{s}_1, \dots, \mathbf{s}_L\}$. This suggests that some kind of vertex search can lead to recovery of \mathbf{A} —the key insight of almost all

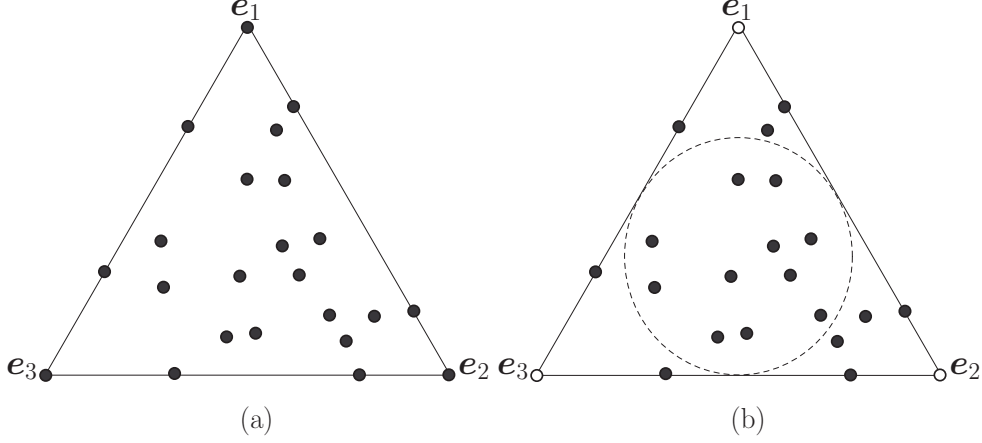


Figure 1: Illustration of geometry of $\mathbf{s}_1, \dots, \mathbf{s}_L$. As an example we consider $N = 3$, and we view the data points by projecting them onto a 2-dimensional space. The solid dark dots are \mathbf{s}_i ’s, and the solid line outlines the boundary of the unit simplex $\text{conv}\{\mathbf{e}_1, \mathbf{e}_2, \mathbf{e}_3\}$. (a) The pure-pixel or separable case, in which $\mathbf{e}_1, \mathbf{e}_2, \mathbf{e}_3$ exist in some of \mathbf{s}_i ’s. (b) A no-pure-pixel or non-separable case in which $\gamma > 1/\sqrt{N-1}$ holds. The dashed line corresponds to a ball $(1/\sqrt{N-1})\mathcal{B}_N$, and is contained in $\text{conv}\{\mathbf{s}_1, \dots, \mathbf{s}_L\}$ as one can see.

algorithms in this framework. The beauty of pure-pixel search or separable NMF is that under the pure-pixel assumption, SSMF can be accomplished either via simple algorithms [1, 25] or via convex optimization [21, 22, 24, 28, 44]. Also, as shown in the aforementioned references, some of these algorithms are supported by theoretical analyses in terms of guarantees on recovery accuracies.

However, a question that has previously puzzled researchers is whether recovery of \mathbf{A} is possible without the pure-pixel assumption. This leads to another framework that hinges on minimum volume enclosing simplex (MVES)—a notion conceived first by Craig in the HU context [20] and an idea that can be traced back to the 1980’s [27]. The idea is to solve an MVES problem

$$\begin{aligned} \min_{\mathbf{b}_1, \dots, \mathbf{b}_N \in \mathbb{R}^M} \quad & \text{vol}(\text{conv}\{\mathbf{b}_1, \dots, \mathbf{b}_N\}) \\ \text{s.t. } & \mathbf{x}_i \in \text{conv}\{\mathbf{b}_1, \dots, \mathbf{b}_N\}, \quad i = 1, \dots, L, \end{aligned} \quad (1)$$

or its variants. As can be seen in (1) and in the illustration in Figure 2, the goal is to find a simplex that encloses the data points and has the minimum volume. The vertices of the MVES, which is the solution $\mathbf{b}_1, \dots, \mathbf{b}_N$ to Problem (1), then serves as the estimate of \mathbf{A} . MVES is more commonly seen in HU, and most recently the idea has made its way to machine learning [26, 33]. Empirically it has been observed that MVES can achieve good recovery accuracies in the absence of pure pixels, and MVES-based algorithms have often been regarded as tools for resolving instances of “heavily mixed pixels” in HU [34]. Recently, the mystery of whether MVES can provide exact recovery *theoretically* has been answered:

Theorem 1 [38] Define

$$\gamma = \max \{r \leq 1 \mid (\text{conv}\{\mathbf{e}_1, \dots, \mathbf{e}_N\}) \cap (r\mathcal{B}_N) \subseteq \text{conv}\{\mathbf{s}_1, \dots, \mathbf{s}_L\}\}, \quad (2)$$

which is called the uniform pixel purity level. If $N \geq 3$ and

$$\gamma > \frac{1}{\sqrt{N-1}},$$

then the optimal solution to the MVES problem (1) must be given by $\mathbf{a}_1, \dots, \mathbf{a}_N$ or their permutations.

The uniform pixel purity level has elegant geometric interpretations. To give readers some feeling, Figure 1(b) illustrates an instance for which $\gamma > 1/\sqrt{N-1}$ holds, but the pure-pixel assumption does not. Also, note that $\gamma = 1$ corresponds to the pure-pixel case. Interested readers are referred to [38] for more explanations of γ , and [23, 26, 33] for concurrent and more recent results for theoretical MVES recovery. Loosely speaking, the premise in Theorem 1 should have a high probability to satisfy in practice as far as the data points are reasonably well spread.

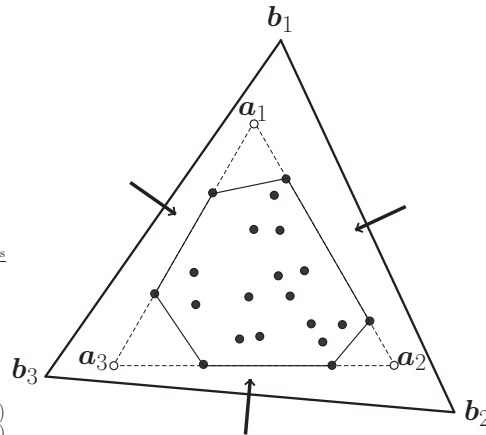


Figure 2: Geometrical illustration of MVES. The way we visualize is the same as in Figure 1. The solid dark dots are the data points $\mathbf{x}_1, \dots, \mathbf{x}_L$, the dashed line outlines where is $\text{conv}\{\mathbf{a}_1, \mathbf{a}_2, \mathbf{a}_3\}$, the solid line inside $\text{conv}\{\mathbf{a}_1, \mathbf{a}_2, \mathbf{a}_3\}$ shows the boundary region of the data convex hull $\text{conv}\{\mathbf{x}_1, \dots, \mathbf{x}_L\}$, and the solid line outside $\text{conv}\{\mathbf{a}_1, \mathbf{a}_2, \mathbf{a}_3\}$ shows a data-enclosing simplex $\text{conv}\{\mathbf{b}_1, \mathbf{b}_2, \mathbf{b}_3\}$ in terms of its boundary region. From this illustration it seems likely that the minimum volume data-enclosing simplex would be $\text{conv}\{\mathbf{a}_1, \mathbf{a}_2, \mathbf{a}_3\}$ itself.

While MVES is appealing in its recovery guarantees, the pursuit of SSMF frameworks is arguably not over. The MVES problem (1) is non-convex and NP-hard in general [43]. Our numerical experience is that the convergence of an MVES algorithm to a good result could depend on the starting point. Hence, from a theoretical viewpoint, it is interesting to study alternative frameworks that can also go beyond the pure-pixel or separability case and can bring new perspective to the no-pure-pixel case—and this is the motivation for our development of the MVIE framework in the next section.

3 Maximum Volume Inscribed Ellipsoid

Let us first describe some facts and our notations with ellipsoids. Any n -dimensional ellipsoid \mathcal{E} in \mathbb{R}^m may be characterized as

$$\mathcal{E} = \mathcal{E}(\mathbf{F}, \mathbf{c}) \triangleq \{\mathbf{F}\boldsymbol{\alpha} + \mathbf{c} \mid \|\boldsymbol{\alpha}\| \leq 1\},$$

for some full column-rank $\mathbf{F} \in \mathbb{R}^{m \times n}$ and $\mathbf{c} \in \mathbb{R}^m$. The volume of an n -dimensional ellipsoid $\mathcal{E}(\mathbf{F}, \mathbf{c})$ is given by

$$\text{vol}(\mathcal{E}(\mathbf{F}, \mathbf{c})) = \rho_n(\det(\mathbf{F}^T \mathbf{F}))^{1/2},$$

where ρ_n denotes the volume of the n -dimensional unit ball [11].

We are interested in an MVIE problem whose aim is to find a maximum volume ellipsoid contained in the convex hull of the data points. For convenience, denote

$$\mathcal{X} = \text{conv}\{\mathbf{x}_1, \dots, \mathbf{x}_L\}$$

to be the convex hull of the data points. As a basic result one can show that

$$\dim \mathcal{X} = \dim(\text{aff}\{\mathbf{x}_1, \dots, \mathbf{x}_L\}) = \dim(\text{aff}\{\mathbf{a}_1, \dots, \mathbf{a}_N\}) = N - 1; \quad (3)$$

note that the second equality is due to $\text{aff}\{\mathbf{x}_1, \dots, \mathbf{x}_L\} = \text{aff}\{\mathbf{a}_1, \dots, \mathbf{a}_N\}$ under (A3), which was proved in [14, 16]. Hence we also restrict the dimension of the ellipsoid to be $N - 1$, and the MVIE problem is formulated as

$$\begin{aligned} & \max_{\mathbf{F}, \mathbf{c}} \det(\mathbf{F}^T \mathbf{F}) \\ & \text{s.t. } \mathcal{E}(\mathbf{F}, \mathbf{c}) \subseteq \mathcal{X}, \end{aligned} \quad (4)$$

where $\mathbf{F} \in \mathbb{R}^{M \times (N-1)}$, $\mathbf{c} \in \mathbb{R}^{M,1}$. We should describe our intuition: As depicted in Figure 3, the MVIE and the data convex hull \mathcal{X} have contact points on their boundaries (in the relative sense). Such contact points may provide a clue on how we may recover \mathbf{A} .

The following theorem describes the main result of this paper.

Theorem 2 Suppose that $N \geq 3$ and $\gamma > 1/\sqrt{N-1}$. The MVIE, or the optimal ellipsoid of Problem (4), is uniquely given by

$$\mathcal{E}^* = \mathcal{E}\left(\frac{1}{\sqrt{N(N-1)}}\mathbf{A}\mathbf{C}, \bar{\mathbf{a}}\right), \quad (5)$$

where $\mathbf{C} \in \mathbb{R}^{N \times (N-1)}$ is any semi-unitary matrix such that $\mathbf{C}^T \mathbf{1} = \mathbf{0}$, and $\bar{\mathbf{a}} = \frac{1}{N} \sum_{i=1}^N \mathbf{a}_i$. Also, there are exactly N contact points between \mathcal{E}^* and $\text{rbd } \mathcal{X}$, that is,

$$\mathcal{E}^* \cap (\text{rbd } \mathcal{X}) = \{\mathbf{q}_1, \dots, \mathbf{q}_N\}, \quad (6)$$

and those contact points are given by

$$\mathbf{q}_i = \frac{1}{N-1} \sum_{j \neq i} \mathbf{a}_j. \quad (7)$$

¹Notice that we do not constrain \mathbf{F} to be of full column rank in Problem (4) for the following reasons. First, it can be verified that a feasible $\mathcal{E}(\mathbf{F}, \mathbf{c})$ with \mathbf{F} being of full column rank always exists if $\dim \mathcal{X} = N - 1$. Second, if \mathbf{F} does not have full column rank then $\det(\mathbf{F}^T \mathbf{F}) = 0$.

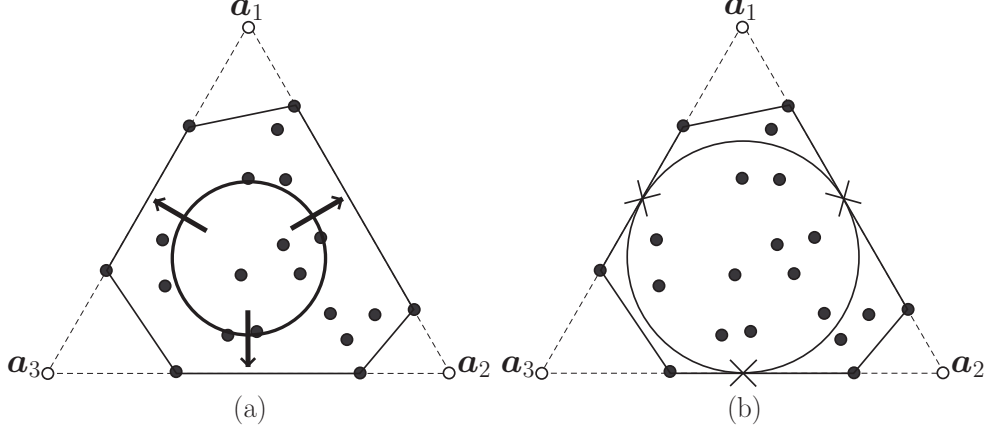


Figure 3: Geometrical illustration of MVIE. The way we visualize is the same as in Figure 2. In the subfigure (a), the circle depicts an ellipsoid inscribed in $\text{conv}\{\mathbf{x}_1, \dots, \mathbf{x}_L\}$. The subfigure in (b) shows a possible scenario for which the MVIE has contact points with $\text{conv}\{\mathbf{x}_1, \dots, \mathbf{x}_L\}$; those contact points are marked by “ \times ”.

Theorem 2 gives a vital implication on a condition under which we can leverage MVIE to exactly recover \mathbf{A} . Consider the following corollary as a direct consequence of Theorem 2.

Corollary 1 *Under the premises of $N \geq 3$ and $\gamma > 1/\sqrt{N-1}$, we can exactly recover \mathbf{A} by solving the MVIE problem (4), finding the contact points \mathbf{q}_i ’s in (6), and reconstructing \mathbf{a}_i ’s either via*

$$\mathbf{a}_i = N\bar{\mathbf{a}} - (N-1)\mathbf{q}_i, \quad i = 1, \dots, N,$$

or via

$$\mathbf{a}_i = \sum_{j=1}^N \mathbf{q}_j - (N-1)\mathbf{q}_i, \quad i = 1, \dots, N.$$

Hence, we have shown a new and provably correct SSMF framework via MVIE. Very coincidentally and beautifully, the sufficient exact recovery condition of this MVIE framework happens to be identical to that of the MVES framework (cf. Theorem 1)—which suggests that MVIE should be as powerful as MVES in a fundamental sense.

In the next section we will describe the proof of Theorem 2. We will also demonstrate the feasibility of the MVIE framework by building an algorithm for it, and then testing it through numerical experiments; these will be considered in Sections 5–6.

4 Proof of Theorem 2

Before we give the full proof of Theorem 2, we should briefly mention the insight behind. At the heart of our proof is John’s theorem for MVIE characterization, which is described as follows.

Theorem 3 [32] *Let $\mathcal{T} \subset \mathbb{R}^n$ be a compact convex set with non-empty interior. The following two statements are equivalent.*

(a) The n -dimensional ellipsoid of maximum volume contained in \mathcal{T} is uniquely given by \mathcal{B}_n .

(b) $\mathcal{B}_n \subseteq \mathcal{T}$ and there exist points $\mathbf{u}_1, \dots, \mathbf{u}_r \in \mathcal{B}_n \cap (\text{bd } \mathcal{T})$, with $r \geq n + 1$, such that

$$\sum_{i=1}^r \lambda_i \mathbf{u}_i = \mathbf{0}, \quad \sum_{i=1}^r \lambda_i \mathbf{u}_i \mathbf{u}_i^T = \mathbf{I},$$

for some $\lambda_1, \dots, \lambda_r > 0$.

There are however challenges to be overcome. First, John's theorem cannot be directly applied to our MVIE problem (4) because \mathcal{X} does not have an interior (although \mathcal{X} has non-empty relative interior). Second, John's theorem does not tell us how to identify the contact points \mathbf{u}_i 's—which we will have to find out. Third, our result in Theorem 2 is stronger in the sense that we characterize the set of *all* the contact points, and this will require some extra work.

The proof of Theorem 2 is divided into three parts and described in the following subsections. Before we proceed, let us define some specific notations that will be used throughout the proof. We will denote an affine set by

$$\mathcal{A}(\Phi, \mathbf{b}) \triangleq \{\Phi\alpha + \mathbf{b} \mid \alpha \in \mathbb{R}^n\},$$

for some $\Phi \in \mathbb{R}^{m \times n}$, $\mathbf{b} \in \mathbb{R}^n$. In fact, any affine set \mathcal{A} in \mathbb{R}^m of $\dim \mathcal{A} = n$ may be represented by $\mathcal{A} = \mathcal{A}(\Phi, \mathbf{b})$ for some full column rank $\Phi \in \mathbb{R}^{m \times n}$ and $\mathbf{b} \in \mathbb{R}^m$. Also, we let $\mathbf{C} \in \mathbb{R}^{N \times (N-1)}$ denote any matrix such that

$$\mathbf{C}^T \mathbf{C} = \mathbf{I}, \quad \mathbf{C}^T \mathbf{1} = \mathbf{0},$$

and we let

$$\mathbf{d} = \frac{1}{N} \mathbf{1} \in \mathbb{R}^N.$$

4.1 Dimensionality Reduction

Our first task is to establish an equivalent MVIE transformation result.

Proposition 1 *Represent the affine hull $\text{aff}\{\mathbf{x}_1, \dots, \mathbf{x}_L\}$ by*

$$\text{aff}\{\mathbf{x}_1, \dots, \mathbf{x}_L\} = \mathcal{A}(\Phi, \mathbf{b}) \tag{8}$$

for some full column rank $\Phi \in \mathbb{R}^{M \times (N-1)}$ and $\mathbf{b} \in \mathbb{R}^M$. Let

$$\mathbf{x}'_i = \Phi^\dagger(\mathbf{x}_i - \mathbf{b}), \quad i = 1, \dots, L, \quad \mathcal{X}' = \text{conv}\{\mathbf{x}'_1, \dots, \mathbf{x}'_L\} \subset \mathbb{R}^{N-1}.$$

The MVIE problem (4) is equivalent to

$$\begin{aligned} & \max_{\mathbf{F}', \mathbf{c}'} |\det(\mathbf{F}')|^2 \\ & \text{s.t. } \mathcal{E}(\mathbf{F}', \mathbf{c}') \subseteq \mathcal{X}', \end{aligned} \tag{9}$$

where $\mathbf{F}' \in \mathbb{R}^{(N-1) \times (N-1)}$, $\mathbf{c}' \in \mathbb{R}^{N-1}$. In particular, the following properties hold:

(a) If (\mathbf{F}, \mathbf{c}) is a feasible (resp., optimal) solution to Problem (4), then

$$(\mathbf{F}', \mathbf{c}') = (\Phi^\dagger \mathbf{F}, \Phi^\dagger(\mathbf{c} - \mathbf{b})) \tag{10}$$

is a feasible (resp., optimal) solution to Problem (9).

(b) If $(\mathbf{F}', \mathbf{c}')$ is a feasible (resp., optimal) solution to Problem (9), then

$$(\mathbf{F}, \mathbf{c}) = (\Phi \mathbf{F}', \Phi \mathbf{c}' + \mathbf{b}) \quad (11)$$

is a feasible (resp., optimal) solution to Problem (4).

(c) The set \mathcal{X}' has non-empty interior.

(d) Let (\mathbf{F}, \mathbf{c}) be a feasible solution to Problem (4), and let $(\mathbf{F}', \mathbf{c}')$ be given by (10); or, let $(\mathbf{F}', \mathbf{c}')$ be a feasible solution to Problem (9), and let (\mathbf{F}, \mathbf{c}) be given by (11). Denote $\mathcal{E} = \mathcal{E}(\mathbf{F}, \mathbf{c})$ and $\mathcal{E}' = \mathcal{E}(\mathbf{F}', \mathbf{c}')$. Then

$$\begin{aligned} \mathbf{q} \in \mathcal{E} \cap (\text{rbd } \mathcal{X}) &\implies \mathbf{q}' = \Phi^\dagger(\mathbf{q} - \mathbf{b}) \in \mathcal{E}' \cap (\text{bd } \mathcal{X}'), \\ \mathbf{q}' \in \mathcal{E}' \cap (\text{bd } \mathcal{X}') &\implies \mathbf{q} = \Phi \mathbf{q}' + \mathbf{b} \in \mathcal{E} \cap (\text{rbd } \mathcal{X}). \end{aligned}$$

The above result is a dimensionality reduction (DR) result where we equivalently transform the MVIE problem from a higher dimension space (specifically, \mathbb{R}^M) to a lower dimensional space (specifically, \mathbb{R}^{N-1}). It has the same flavor as the so-called affine set fitting result in [14, 16], which is also identical to principal component analysis. This DR result will be used again when we develop an algorithm for MVIE in later sections. We relegate the proof of Proposition 1 to Appendix A.

Now, we construct an equivalent MVIE problem via a specific choice of (Φ, \mathbf{b}) . It has been shown that under (A3),

$$\text{aff}\{\mathbf{x}_1, \dots, \mathbf{x}_L\} = \text{aff}\{\mathbf{a}_1, \dots, \mathbf{a}_N\}; \quad (12)$$

see [14, 16]. Also, consider the following fact.

Fact 1 [38] The affine hull of all unit vectors $\mathbf{e}_1, \dots, \mathbf{e}_N$ in \mathbb{R}^N can be characterized as

$$\text{aff}\{\mathbf{e}_1, \dots, \mathbf{e}_N\} = \mathcal{A}(\mathbf{C}, \mathbf{d}).$$

Applying Fact 1 to (12) yields

$$\text{aff}\{\mathbf{x}_1, \dots, \mathbf{x}_L\} = \mathcal{A}(\mathbf{AC}, \mathbf{Ad}).$$

By choosing $(\Phi, \mathbf{b}) = (\mathbf{AC}, \mathbf{Ad})$ and applying Proposition 1, we obtain an equivalent MVIE problem in (9) that has

$$\mathbf{x}_i = \mathbf{ACx}'_i + \mathbf{Ad}, \quad i = 1, \dots, L.$$

The above equation can be simplified. By plugging the model $\mathbf{x}_i = \mathbf{As}_i$ into the above equation, we get $\mathbf{s}_i = \mathbf{Cx}'_i + \mathbf{d}$; and using the properties $\mathbf{C}^T \mathbf{C} = \mathbf{I}$ and $\mathbf{C}^T \mathbf{d} = \mathbf{0}$ we further get $\mathbf{x}'_i = \mathbf{C}^T \mathbf{s}_i$. By changing the notation \mathcal{X}' to \mathcal{S}' , and \mathbf{x}'_i to \mathbf{s}'_i , we rewrite the equivalent MVIE problem (9) as

$$\begin{aligned} \max_{\mathbf{F}', \mathbf{c}'} |\det(\mathbf{F}')|^2 \\ \text{s.t. } \mathcal{E}(\mathbf{F}', \mathbf{c}') \subseteq \mathcal{S}', \end{aligned} \quad (13)$$

where we again have $\mathbf{F}' \in \mathbb{R}^{(N-1) \times (N-1)}$, $\mathbf{c}' \in \mathbb{R}^{N-1}$; \mathcal{S}' is given by $\mathcal{S}' = \text{conv}\{\mathbf{s}'_1, \dots, \mathbf{s}'_L\}$ with

$$\mathbf{s}'_i = \mathbf{C}^T \mathbf{s}_i, \quad i = 1, \dots, L.$$

Furthermore, note that \mathcal{S}' has non-empty interior; cf. Statement (c) of Proposition 1.

4.2 Solving the MVIE via John's Theorem

Next, we apply John's theorem to the equivalent MVIE problem in (13). It would be helpful to describe the result from a big picture viewpoint first. For convenience, let

$$\beta = \frac{1}{\sqrt{N(N-1)}}$$

and

$$\mathbf{q}'_i = \frac{1}{N-1} \sum_{j \neq i} \mathbf{C}^T \mathbf{e}_j, \quad i = 1, \dots, N.$$

We will show that the optimal ellipsoid to Problem (13) is uniquely given by $\beta\mathcal{B}_{N-1}$, and that $\mathbf{q}'_1, \dots, \mathbf{q}'_N$ lie in $(\beta\mathcal{B}_{N-1}) \cap (\text{bd } \mathcal{S}')$; the underlying premise is $\gamma \geq 1/\sqrt{N-1}$. Subsequently, by the equivalence properties in Proposition 1, and by $\beta\mathcal{B}_{N-1} = \mathcal{E}(\beta\mathbf{I}, \mathbf{0})$, we have

$$\mathcal{E}(\beta\mathbf{AC}, \mathbf{Ad}) = \mathcal{E}^*$$

as the optimal ellipsoid of our original MVIE problem (4); also, we have

$$\mathbf{q}_i = \mathbf{AC}\mathbf{q}'_i + \mathbf{Ad} \in \mathcal{E}^* \cap (\text{rbd } \mathcal{X}), \quad i = 1, \dots, N.$$

Furthermore, it will be shown that \mathbf{q}_i can be reduced to $\mathbf{q}_i = \frac{1}{N-1} \sum_{j \neq i} \mathbf{a}_j$. Hence, except for the claim $\{\mathbf{q}_1, \dots, \mathbf{q}_N\} = \mathcal{E}^* \cap (\text{rbd } \mathcal{X})$, we see all the results in Theorem 2.

Now, we show the more detailed parts of the proof.

Step 1: Let us assume $\beta\mathcal{B}_{N-1} \subseteq \mathcal{S}'$ and $\mathbf{q}'_i \in (\beta\mathcal{B}_{N-1}) \cap (\text{bd } \mathcal{S}')$ for all i ; we will come back to this later. The aim here is to verify that $\beta\mathcal{B}_{N-1}$ and $\mathbf{q}'_1, \dots, \mathbf{q}'_N$ satisfy the MVIE conditions in John's theorem. Since $\mathbf{C}^T \mathbf{1} = \mathbf{0}$, we can simplify \mathbf{q}'_i to

$$\mathbf{q}'_i = \frac{1}{N-1} \mathbf{C}^T (\mathbf{1} - \mathbf{e}_i) = -\frac{1}{N-1} \mathbf{C}^T \mathbf{e}_i.$$

Consequently, one can verify that

$$\begin{aligned} (N-1)^2 \sum_{i=1}^N \mathbf{q}'_i &= -(N-1)^2 \mathbf{C}^T \mathbf{1} = \mathbf{0}, \\ (N-1)^2 \sum_{i=1}^N (\mathbf{q}'_i)(\mathbf{q}'_i)^T &= \mathbf{C}^T \left(\sum_{i=1}^N \mathbf{e}_i \mathbf{e}_i^T \right) \mathbf{C} = \mathbf{C}^T \mathbf{I} \mathbf{C} = \mathbf{I}, \end{aligned}$$

which are the MVIE conditions of John's theorem; see Statement (b) of Theorem 3. Hence, $\beta\mathcal{B}_{N-1}$ is the unique maximum volume ellipsoid contained in \mathcal{S}' .

Step 2: We verify that $\beta\mathcal{B}_{N-1} \subseteq \mathcal{S}'$ if $\gamma \geq 1/\sqrt{N-1}$. The verification requires another equivalent MVIE problem, given as follows:

$$\begin{aligned} \max_{\mathbf{F}, \mathbf{c}} \quad & \det(\mathbf{F}^T \mathbf{F}) \\ \text{s.t. } & \mathcal{E}(\mathbf{F}, \mathbf{c}) \subseteq \mathcal{S}, \end{aligned} \tag{14}$$

where

$$\mathcal{S} = \text{conv}\{\mathbf{s}_1, \dots, \mathbf{s}_L\},$$

and with a slight abuse of notations we redefine $\mathbf{F} \in \mathbb{R}^{N \times (N-1)}$, $\mathbf{c} \in \mathbb{R}^N$. Using the same result in the previous subsection, it can be readily shown that Problem (14) is equivalent to Problem (13) under $(\Phi, \mathbf{b}) = (\mathbf{C}, \mathbf{d})$. Let

$$\mathcal{E} = \mathcal{E}(\beta\mathbf{C}, \mathbf{d}), \quad \mathcal{E}' = \mathcal{E}(\beta\mathbf{I}, \mathbf{0}) = \beta\mathcal{B}_{N-1}.$$

From Statement (a) of Proposition 1, we have $\mathcal{E} \subseteq \mathcal{S} \implies \mathcal{E}' \subseteq \mathcal{S}'$; thus, we turn to proving $\mathcal{E} \subseteq \mathcal{S}$. Recall from the definition of γ in (2) that

$$(\text{conv}\{\mathbf{e}_1, \dots, \mathbf{e}_N\}) \cap (\gamma\mathcal{B}_N) \subseteq \mathcal{S}. \quad (15)$$

For $\gamma \geq 1/\sqrt{N-1}$, (15) implies

$$(\text{conv}\{\mathbf{e}_1, \dots, \mathbf{e}_N\}) \cap \left(\frac{1}{\sqrt{N-1}}\mathcal{B}_N\right) \subseteq \mathcal{S}. \quad (16)$$

Consider the following fact.

Fact 2 [38] *The following results hold.*

- (a) $(\text{aff}\{\mathbf{e}_1, \dots, \mathbf{e}_N\}) \cap (r\mathcal{B}_N) = \mathcal{E}\left(\sqrt{r^2 - \frac{1}{N}}\mathbf{C}, \mathbf{d}\right)$ for $r \geq \frac{1}{\sqrt{N}}$;
- (b) $(\text{conv}\{\mathbf{e}_1, \dots, \mathbf{e}_N\}) \cap (r\mathcal{B}_N) = \text{aff}\{\mathbf{e}_1, \dots, \mathbf{e}_N\} \cap (r\mathcal{B}_N)$ for $\frac{1}{\sqrt{N}} < r \leq \frac{1}{\sqrt{N-1}}$.

Applying Fact 2 to the left-hand side of (16) yields

$$(\text{conv}\{\mathbf{e}_1, \dots, \mathbf{e}_N\}) \cap \left(\frac{1}{\sqrt{N-1}}\mathcal{B}_N\right) = \mathcal{E}(\beta\mathbf{C}, \mathbf{d}). \quad (17)$$

Hence, we have $\mathcal{E} = \mathcal{E}(\beta\mathbf{C}, \mathbf{d}) \subseteq \mathcal{S}$, which implies that $\beta\mathcal{B}_{N-1} = \mathcal{E}' \subseteq \mathcal{S}'$.

Step 3: We verify that $\mathbf{q}'_i \in (\beta\mathcal{B}_{N-1}) \cap (\text{bd } \mathcal{S}')$ for all i . Again, the verification is based on the equivalence of Problem (14) and Problem (13) used in Step 2. Let

$$\mathbf{w}_i = \frac{1}{N-1} \sum_{j \neq i} \mathbf{e}_j, \quad i = 1, \dots, N, \quad (18)$$

and let $\mathbf{w}'_i = \mathbf{C}^T(\mathbf{w}_i - \mathbf{d})$ for all i . By Statement (d) of Proposition 1, we have $\mathbf{w}_i \in \mathcal{E} \cap (\text{rbd } \mathcal{S}) \implies \mathbf{w}'_i \in \mathcal{E}' \cap (\text{bd } \mathcal{S}')$. Also, owing to $\mathbf{C}^T \mathbf{d} = \mathbf{0}$, we see that $\mathbf{w}'_i = \mathbf{C}^T(\frac{1}{N-1} \sum_{j \neq i} \mathbf{e}_j) = \mathbf{q}'_i$. Hence, we can focus on showing $\mathbf{w}_i \in \mathcal{E} \cap (\text{rbd } \mathcal{S})$. Since $\mathbf{w}_i \in \text{aff}\{\mathbf{e}_1, \dots, \mathbf{e}_N\} = \mathcal{A}(\mathbf{C}, \mathbf{d})$ (cf. Fact 1), we can represent \mathbf{w}_i by

$$\mathbf{w}_i = \mathbf{C}\mathbf{w}'_i + \mathbf{d}. \quad (19)$$

Using (18), $\mathbf{C}^T \mathbf{C} = \mathbf{I}$ and $\mathbf{C}^T \mathbf{d} = \mathbf{0}$, one can verify that

$$\frac{1}{N-1} = \|\mathbf{w}_i\|^2 = \|\mathbf{C}\mathbf{w}'_i\|^2 + \|\mathbf{d}\|^2 = \|\mathbf{w}'_i\|^2 + \frac{1}{N},$$

which is equivalent to $\|\mathbf{w}'_i\| = \beta$. We thus have $\mathbf{w}_i \in \mathcal{E}(\beta\mathbf{C}, \mathbf{d}) = \mathcal{E}$. Since $\mathcal{E} \subseteq \mathcal{S}$ (which is shown in Step 2), we also have $\mathbf{w}_i \in \mathcal{S}$. The vector \mathbf{w}_i has $[\mathbf{w}_i]_i = 0$, and as a result \mathbf{w}_i must not lie in $\text{ri } \mathcal{S}$. It follows that $\mathbf{w}_i \in \text{rbd } \mathcal{S}$.

Step 4: Steps 1–3 essentially prove all the key components of the big picture proof described in the beginning of this subsection. In this last step, we show the remaining result, namely, $\mathbf{q}_i = \mathbf{A}\mathbf{C}\mathbf{q}'_i + \mathbf{A}\mathbf{d} = \frac{1}{N-1} \sum_{j \neq i} \mathbf{a}_j$. In Step 3, we see from $\mathbf{w}'_i = \mathbf{q}'_i$ and (18)–(19) that $\mathbf{C}\mathbf{q}'_i + \mathbf{d} = \frac{1}{N-1} \sum_{j \neq i} \mathbf{e}_j$. Plugging this result into \mathbf{q}_i yields the desired result.

4.3 On the Number of Contact Points

Our final task is to prove that $\{\mathbf{q}_1, \dots, \mathbf{q}_N\} = \mathcal{E}^* \cap (\text{rbd } \mathcal{X})$; note that the previous proof allows us only to say that $\{\mathbf{q}_1, \dots, \mathbf{q}_N\} \subseteq \mathcal{E}^* \cap (\text{rbd } \mathcal{X})$. We use the equivalent MVIE problem (14) to help us solve the problem. Again, let $\mathcal{E} = \mathcal{E}(\beta\mathbf{C}, \mathbf{d})$ for convenience. The crux is to show that

$$\mathbf{w} \in \mathcal{E} \cap (\text{rbd } \mathcal{S}) \implies \mathbf{w} = \mathbf{w}_i \text{ for some } i \in \{1, \dots, N\}, \quad (20)$$

where \mathbf{w}_i 's have been defined in (18); the premise is $\gamma > 1/\sqrt{N-1}$. By following the above development, especially, the equivalence results of Problems (14) and (13) and those of Problems (4) and (13), it can be verified that (20) is equivalent to

$$\mathbf{q} \in \mathcal{E}^* \cap (\text{rbd } \mathcal{X}) \implies \mathbf{q} = \mathbf{q}_i \text{ for some } i \in \{1, \dots, N\},$$

which completes the proof of $\{\mathbf{q}_1, \dots, \mathbf{q}_N\} = \mathcal{E}^* \cap (\text{rbd } \mathcal{X})$. We describe the proof of (20) as follows.

Step 1: First, we show the following implication under $\gamma > 1/\sqrt{N-1}$:

$$\mathbf{w} \in \mathcal{E} \cap (\text{rbd } \mathcal{S}) \implies \mathbf{w} \in \mathcal{E} \cap (\text{rbd}(\text{conv}\{\mathbf{e}_1, \dots, \mathbf{e}_N\})). \quad (21)$$

The proof is as follows. Let

$$\mathcal{R}(\gamma) = (\text{conv}\{\mathbf{e}_1, \dots, \mathbf{e}_N\}) \cap (\gamma\mathcal{B}_N),$$

and note from (15)–(17) that

$$\mathcal{E} \subseteq \mathcal{R}(\gamma) \subseteq \mathcal{S} \quad (22)$$

holds for $\gamma \geq 1/\sqrt{N-1}$. It can be seen or easily verified from the previous development that

$$\text{aff } \mathcal{E} = \text{aff } \mathcal{S} = \text{aff}(\text{conv}\{\mathbf{e}_1, \dots, \mathbf{e}_N\}) = \text{aff}\{\mathbf{e}_1, \dots, \mathbf{e}_N\} = \mathcal{A}(\mathbf{C}, \mathbf{d}). \quad (23)$$

Also, by applying (23) to (22), we get $\text{aff}(\mathcal{R}(\gamma)) = \mathcal{A}(\mathbf{C}, \mathbf{d})$. It is then immediate that

$$\text{ri}(\mathcal{R}(\gamma)) \subseteq \text{ri } \mathcal{S}. \quad (24)$$

From (22)–(24) we observe that

$$\mathbf{w} \in \mathcal{E}, \mathbf{w} \in \text{rbd } \mathcal{S} \implies \mathbf{w} \in \mathcal{R}(\gamma), \mathbf{w} \notin \text{ri}(\mathcal{R}(\gamma)) \implies \mathbf{w} \in \text{rbd}(\mathcal{R}(\gamma)). \quad (25)$$

Let us further examine the right-hand side of the above equation. For $\gamma > 1/\sqrt{N}$, we can write

$$\begin{aligned} \mathcal{R}(\gamma) &= (\text{conv}\{\mathbf{e}_1, \dots, \mathbf{e}_N\}) \cap (\text{aff}\{\mathbf{e}_1, \dots, \mathbf{e}_N\} \cap (\gamma\mathcal{B}_N)) \\ &= (\text{conv}\{\mathbf{e}_1, \dots, \mathbf{e}_N\}) \cap \left(\mathcal{E} \left(\sqrt{\gamma^2 - \frac{1}{N}} \mathbf{C}, \mathbf{d} \right) \right), \end{aligned}$$

where the second equality is due to Fact 2.(a). It follows that

$$\mathbf{w} \in \text{rbd}(\mathcal{R}(\gamma)) \implies \mathbf{w} \in \text{rbd}(\text{conv}\{\mathbf{e}_1, \dots, \mathbf{e}_N\}) \text{ or } \mathbf{w} \in \text{rbd}\left(\mathcal{E}\left(\sqrt{\gamma^2 - \frac{1}{N}}\mathbf{C}, \mathbf{d}\right)\right). \quad (26)$$

However, for $\gamma > 1/\sqrt{N-1}$, we have

$$\mathbf{w} \in \mathcal{E} = \mathcal{E}(\beta\mathbf{C}, \mathbf{d}) = \mathcal{E}\left(\sqrt{\frac{1}{N-1} - \frac{1}{N}}\mathbf{C}, \mathbf{d}\right) \implies \mathbf{w} \notin \text{rbd}\left(\mathcal{E}\left(\sqrt{\gamma^2 - \frac{1}{N}}\mathbf{C}, \mathbf{d}\right)\right). \quad (27)$$

By combining (25), (26) and (27), we obtain (21).

Step 2: Second, we show that

$$\mathbf{w} \in \mathcal{E} \cap (\text{rbd}(\text{conv}\{\mathbf{e}_1, \dots, \mathbf{e}_N\})) \implies \mathbf{w} = \mathbf{w}_i \text{ for some } i \in \{1, \dots, N\}. \quad (28)$$

The proof is as follows. The relative boundary of $\text{conv}\{\mathbf{e}_1, \dots, \mathbf{e}_N\}$ can be expressed as

$$\text{rbd}(\text{conv}\{\mathbf{e}_1, \dots, \mathbf{e}_N\}) = \bigcup_{i=1}^N \mathcal{F}_i$$

where

$$\mathcal{F}_i = \{\mathbf{s} \in \mathbb{R}^N \mid \mathbf{s} \geq \mathbf{0}, \mathbf{1}^T \mathbf{s} = 1, s_i = 0\}. \quad (29)$$

It follows that

$$\mathbf{w} \in \mathcal{E} \cap (\text{rbd}(\text{conv}\{\mathbf{e}_1, \dots, \mathbf{e}_N\})) \implies \mathbf{w} \in \mathcal{E} \cap \mathcal{F}_i \text{ for some } i \in \{1, \dots, N\}.$$

Recall $\mathbf{w}_i = \frac{1}{N-1} \sum_{j \neq i} \mathbf{e}_j$. By the Cauchy-Schwartz inequality, any $\mathbf{w} \in \mathcal{F}_i$ must satisfy

$$\|\mathbf{w}\| = \sqrt{N-1} \|\mathbf{w}_i\| \|\mathbf{w}\| \geq \sqrt{N-1} \mathbf{w}_i^T \mathbf{w} = \frac{1}{\sqrt{N-1}}.$$

Also, the above equality holds (for $\mathbf{w} \in \mathcal{F}_i$) if and only if $\mathbf{w} = \mathbf{w}_i$. On the other hand, it can be verified that any $\mathbf{w} \in \mathcal{E}$ must satisfy $\|\mathbf{w}\| \leq 1/\sqrt{N-1}$; see (22). Hence, any $\mathbf{w} \in \mathcal{E} \cap \mathcal{F}_i$ must be given by $\mathbf{w} = \mathbf{w}_i$, and applying this result to (29) leads to (28).

Finally, by (21) and (28), the desired result in (20) is obtained.

5 An SSMF Algorithm Induced from MVIE

In this section we use the MVIE framework developed in the previous sections to derive an SSMF algorithm. Specifically, we follow the recovery procedure in Corollary 1. As can be seen in Corollary 1, the main problem is to solve the MVIE problem in (4).

To solve Problem (4), we first consider DR. The required tool has been built in Proposition 1: If we can find a 2-tuple $(\Phi, \mathbf{b}) \in \mathbb{R}^{M \times (N-1)} \times \mathbb{R}^M$ such that $\text{aff}\{\mathbf{x}_1, \dots, \mathbf{x}_L\} = \mathcal{A}(\Phi, \mathbf{b})$, then the MVIE problem (4) can be equivalently transformed to Problem (9), restated here for convenience as follows:

$$\begin{aligned} & \max_{\mathbf{F}', \mathbf{c}'} |\det(\mathbf{F}')|^2 \\ & \text{s.t. } \mathcal{E}(\mathbf{F}', \mathbf{c}') \subseteq \mathcal{X}' = \text{conv}\{\mathbf{x}'_1, \dots, \mathbf{x}'_L\}, \end{aligned} \quad (30)$$

where $(\mathbf{F}', \mathbf{c}') \in \mathbb{R}^{(N-1) \times (N-1)} \times \mathbb{R}^{N-1}$, and $\mathbf{x}'_i = \Phi^\dagger(\mathbf{x}_i - \mathbf{b})$, $i = 1, \dots, L$ are the dimensionality-reduced data points. Specifically, recall that if $(\mathbf{F}', \mathbf{c}')$ is an optimal solution to Problem (30) then $(\mathbf{F}, \mathbf{c}) = (\Phi \mathbf{F}', \Phi \mathbf{F}' + \mathbf{c})$ is an optimal solution to Problem (4); if $\mathbf{q}' \in (\mathcal{E}(\mathbf{F}', \mathbf{c}')) \cap (\text{bd } \mathcal{X}')$, then $\mathbf{q} = \Phi \mathbf{q}' + \mathbf{b} \in (\mathcal{E}(\mathbf{F}, \mathbf{c})) \cap (\text{rbd } \mathcal{X})$ is one of the desired contact points in (7). The problem is to find one such (Φ, \mathbf{b}) from the data. According to [14], we can extract (Φ, \mathbf{b}) from the data using affine set fitting; it is given by $\mathbf{b} = \frac{1}{L} \sum_{n=1}^L \mathbf{x}_n$ and by having columns of Φ to be first $N - 1$ principal left-singular vectors of the matrix $[\mathbf{x}_1 - \mathbf{b}, \dots, \mathbf{x}_L - \mathbf{b}]$.

Next, we show how Problem (30) can be recast as a convex problem. To do so, we consider representing \mathcal{X}' in polyhedral form, that is,

$$\mathcal{X}' = \bigcap_{i=1}^K \{\mathbf{x} \mid \mathbf{g}_i^T \mathbf{x}_i \leq h_i\},$$

for some positive integer K and for some $(\mathbf{g}_i, h_i) \in \mathbb{R}^{N-1} \times \mathbb{R}$, $i = 1, \dots, K$, with $\|\mathbf{g}_i\| = 1$ without loss of generality. Such a conversion is called facet enumeration in the literature [12], and in practice $(\mathbf{g}_i, h_i)_{i=1}^K$ may be obtained by calling an off-the-shelf facet enumeration algorithm such as QuickHull [4]. Using the polyhedral representation of \mathcal{X}' , Problem (30) can be reformulated as a log determinant maximization problem subject to second-order cone (SOC) constraints [11]. Without loss of generality, assume that \mathbf{F}' is symmetric and positive semidefinite. By noting $\det(\mathbf{F}') \geq 0$ and the equivalence

$$\begin{aligned} \mathcal{E}(\mathbf{F}', \mathbf{c}') \subseteq \bigcap_{i=1}^K \{\mathbf{x} \mid \mathbf{g}_i^T \mathbf{x}_i \leq h_i\} &\iff \sup_{\|\boldsymbol{\alpha}\| \leq 1} \mathbf{g}_i^T (\mathbf{F}' \boldsymbol{\alpha} + \mathbf{c}') \leq h_i, \quad i = 1, \dots, K, \\ &\iff \|\mathbf{F}' \mathbf{g}_i\| + \mathbf{g}_i^T \mathbf{c}' \leq h_i, \quad i = 1, \dots, K; \end{aligned} \quad (31)$$

(see, e.g., [11]), Problem (30) can be rewritten as

$$\begin{aligned} \max_{\mathbf{F}' \in \mathbb{S}_+^{N-1}, \mathbf{c}' \in \mathbb{R}^{N-1}} \quad &\log \det(\mathbf{F}') \\ \text{s.t.} \quad &\|\mathbf{F}' \mathbf{g}_i\| + \mathbf{g}_i^T \mathbf{c}' \leq h_i, \quad i = 1, \dots, K. \end{aligned} \quad (32)$$

The above problem is convex and can be readily solved by calling general-purpose convex optimization software such as CVX [31]. We also custom-derive a fast first-order algorithm for handling Problem (32). The algorithm is described in Appendix B.

The aspect of MVIE optimization is complete. However, we should also mention how we obtain the contact points $\mathbf{q}_1, \dots, \mathbf{q}_N$ in (6)–(7) as they play a key role in reconstructing $\mathbf{a}_1, \dots, \mathbf{a}_N$; cf. Corollary 1. It can be further shown from (31) that

$$\mathbf{q}' \in (\mathcal{E}(\mathbf{F}', \mathbf{c}')) \cap (\text{bd } \mathcal{X}') \iff \mathbf{q}' = \mathbf{F}' \left(\frac{\mathbf{F}' \mathbf{g}_i}{\|\mathbf{F}' \mathbf{g}_i\|} \right) + \mathbf{c}', \quad \|\mathbf{F}' \mathbf{g}_i\| + \mathbf{g}_i^T \mathbf{c}' = h_i, \quad (33)$$

for some $i = 1, \dots, K$.

Hence, after solving Problem (32), we can use the condition on the right-hand side of (33) to identify the collection of all contact points $\mathbf{q}'_1, \dots, \mathbf{q}'_N$. Then, we use the relation $\mathbf{q}_i = \Phi \mathbf{q}'_i + \mathbf{b}$ to construct $\mathbf{q}_1, \dots, \mathbf{q}_N$. Our MVIE algorithm is summarized in Algorithm 1.

Some discussions are as follows.

Algorithm 1 An MVIE Algorithm for Blind Recovery of \mathbf{A}

- 1: **Given** a data matrix $\mathbf{X} \in \mathbb{R}^{M \times L}$ and a model order $N \leq \min\{M, L\}$.
- 2: Obtain the dimension-reduced data $\mathbf{x}'_i = \Phi^\dagger(\mathbf{x}_i - \mathbf{b}), i = 1, \dots, L$, where (Φ, \mathbf{b}) is obtained by affine set fitting [14].
- 3: Use QuickHull [4] or some other off-the-shelf algorithm to enumerate the facets of $\text{conv}\{\mathbf{x}'_1, \dots, \mathbf{x}'_L\}$, i.e., find $(\mathbf{g}_i, h_i)_{i=1}^K$ such that $\text{conv}\{\mathbf{x}'_1, \dots, \mathbf{x}'_L\} = \bigcap_{i=1}^K \{\mathbf{x} \mid \mathbf{g}_i^T \mathbf{x} \leq h_i\}$.
- 4: Solve Problem (32) either via CVX [31] or via Algorithm 2, and store the optimal solution obtained as $(\mathbf{F}', \mathbf{c}')$.
- 5: Compute the contact points
$$\{\mathbf{q}'_1, \dots, \mathbf{q}'_N\} = \left\{ \mathbf{q}' = \mathbf{F}' \left(\frac{\mathbf{F}' \mathbf{g}_i}{\|\mathbf{F}' \mathbf{g}_i\|} \right) + \mathbf{c}' \mid i \in \{1, \dots, K\} \text{ is such that } \|\mathbf{F}' \mathbf{g}_i\| + \mathbf{g}_i^T \mathbf{c}' = h_i \right\}$$
- 6: Compute the contact points $\mathbf{q}_i = \Phi \mathbf{q}'_i + \mathbf{b}, i = 1, \dots, N$.
- 7: Reconstruct $\mathbf{a}_i = \sum_{j=1}^N \mathbf{q}_j - (N-1)\mathbf{q}_i, i = 1, \dots, N$.
- 8: **Output** $\mathbf{A} = [\mathbf{a}_1, \dots, \mathbf{a}_N]$.

1. As can be seen, the two key steps for the proposed MVIE algorithm are to perform facet enumeration and to solve a convex optimization problem. Let us first discuss issues arising from facet enumeration. Facet enumeration is a well-studied problem in the context of computational geometry [12, 13], and one can find off-the-shelf algorithms, such as QuickHull [4] and VERT2CON², that may efficiently process facet enumeration in practice. Our numerical experiment in the next section will show that facet enumeration is not the main complexity overhead of our algorithm in practice; instead, solving the convex problem takes more time. However, it is important to note that facet enumeration is known to be NP-hard in the worst-case sense [5, 10]. Such computational intractability was identified by finding a purposely constructed problem instance [3], which is reminiscent of the carefully constructed Klee-Minty cube for showing the worst-case complexity of the simplex method for linear programming [35]. In practice, one would argue that such worst-case instances do not happen too often. Moreover, the facet enumeration problem is polynomial-time solvable under certain sufficient conditions, such as the so-called “balance condition” [4, Theorem 3.2] and the case of $N = 3$ [19].
2. While the above discussion suggests that MVIE may not be solved in polynomial time, it is based on convex optimization and thus does not suffer from local minima. In comparison, MVES—which enjoys the same sufficient recovery condition as MVIE—may have such issues as we will see in the numerical results in the next section.
3. We should also discuss a minor issue, namely, that of finding the contact points in Step 5 of Algorithm 1. In practice, there may be numerical errors with the MVIE optimization process. Also, data in reality are often noisy. Those errors may result in identification of more than N contact points as our experience suggests. When such instances happen, we mend the problem by clustering the obtained contact points into N points by standard k -means clustering.

²<https://www.mathworks.com/matlabcentral/fileexchange/7895-vert2con-vertices-to-constraints>

6 Numerical Simulation and Discussion

In this section we use numerical simulations to show the viability of the MVIE framework. The application scenario is HU in remote sensing. The data matrix $\mathbf{X} = \mathbf{AS}$ is synthetically generated by following the procedure in [14]. Specifically, the columns $\mathbf{a}_1, \dots, \mathbf{a}_N$ of \mathbf{A} are randomly selected from a library of endmember spectral signatures called the U.S. geological survey (USGS) library [18]. To generate the columns $\mathbf{s}_1, \dots, \mathbf{s}_L$ of \mathbf{S} , we first generate a large pool of Dirichlet distributed random vectors with concentration parameter $\mathbf{1}/N$. Then, we choose $\mathbf{s}_1, \dots, \mathbf{s}_L$ as a subset of such random vectors whose Euclidean norm is less than or equal to a pre-specified number r . In doing so, we use r to control the pixel purity level of the data. In the simulations we set $M = 224, L = 1,000$.

To get some ideas on how the proposed MVIE algorithm works compared to algorithms under other SSMF frameworks, our simulations also include the successive projection algorithm (SPA), SISAL [7] and MVES [14]. SPA is a fast algorithm under the separable NMF or pure-pixel search framework. SISAL and MVES were developed under the MVES framework. We adopt the root-mean-square (RMS) angle error as our recovery performance measure. Given an estimate $\hat{\mathbf{A}}$ of \mathbf{A} from \mathbf{X} , the RMS angle error is defined as

$$\phi = \min_{\pi \in \Pi_N} \sqrt{\frac{1}{N} \sum_{i=1}^N \left[\arccos \left(\frac{\mathbf{a}_i^T \hat{\mathbf{a}}_{\pi_i}}{\|\mathbf{a}_i\| \cdot \|\hat{\mathbf{a}}_{\pi_i}\|} \right) \right]^2},$$

where Π_N denotes the set of all permutations of $\{1, \dots, N\}$. Also, a number of 50 independently generated realizations were used to evaluate the RMS angle error performance on average. All the algorithms are implemented under Mathworks Matlab R2015a, and they were run on a computer with Core-i7-4790K CPU (3.6 GHz CPU speed) and with 16GB RAM.

Figure 4 shows the RMS angle error performance of the various algorithms with respect to the pixel purity level r . In the legend “MVIE-CVX” stands for the implementation of the proposed MVIE algorithm in Algorithm 1 using the general-purpose convex optimization software CVX, while “MVIE-FPGM” the MVIE implementation using the custom-derived algorithm in Algorithm 2 (with $\rho = 150, \epsilon = 2.22 \times 10^{-16}$). We observe that the two MVIE algorithms generally outperform the other algorithms, with MVIE-CVX being slightly better than MVIE-FPGM. However, we will see later that MVIE-FPGM runs a lot faster than MVIE-CVX.

Let us also comment on the performance of the other algorithms. The recovery performance of SPA degrades as the pixel purity level r decreases, and this makes sense because separable NMF or pure-pixel search is based on the separability or pure-pixel assumption, which corresponds to $r = 1$ in our simulations (in a high probability sense). SISAL and MVES are able to provide good recovery when r is not too small, e.g., $r \geq 0.6$ for the case of $N = 5$. By our numerical experience, this may be owing to the fact that SISAL and MVES converge to a stationary point that is not the optimal solution. To further illustrate this, in Figure 5 we show an additional numerical result where we use slightly perturbed versions of the groundtruth $\mathbf{a}_1, \dots, \mathbf{a}_N$ as the initialization and see if MVES and SISAL would converge to a different solution. “SISAL-cheat” and “MVES-cheat” refer to MVES and SISAL run under such cheat initializations, resp.; “SISAL” and “MVES” refer to the original MVES and SISAL, resp. We see from the numerical result that the two can have significant gaps, which verifies that the current MVES-based algorithms can be sensitive to initializations.

Our theoretical development for MVIE assumes the noiseless case. Having said so, it is still interesting to take a look at how MVIE performs in the noisy case. Figure 6 shows the results when

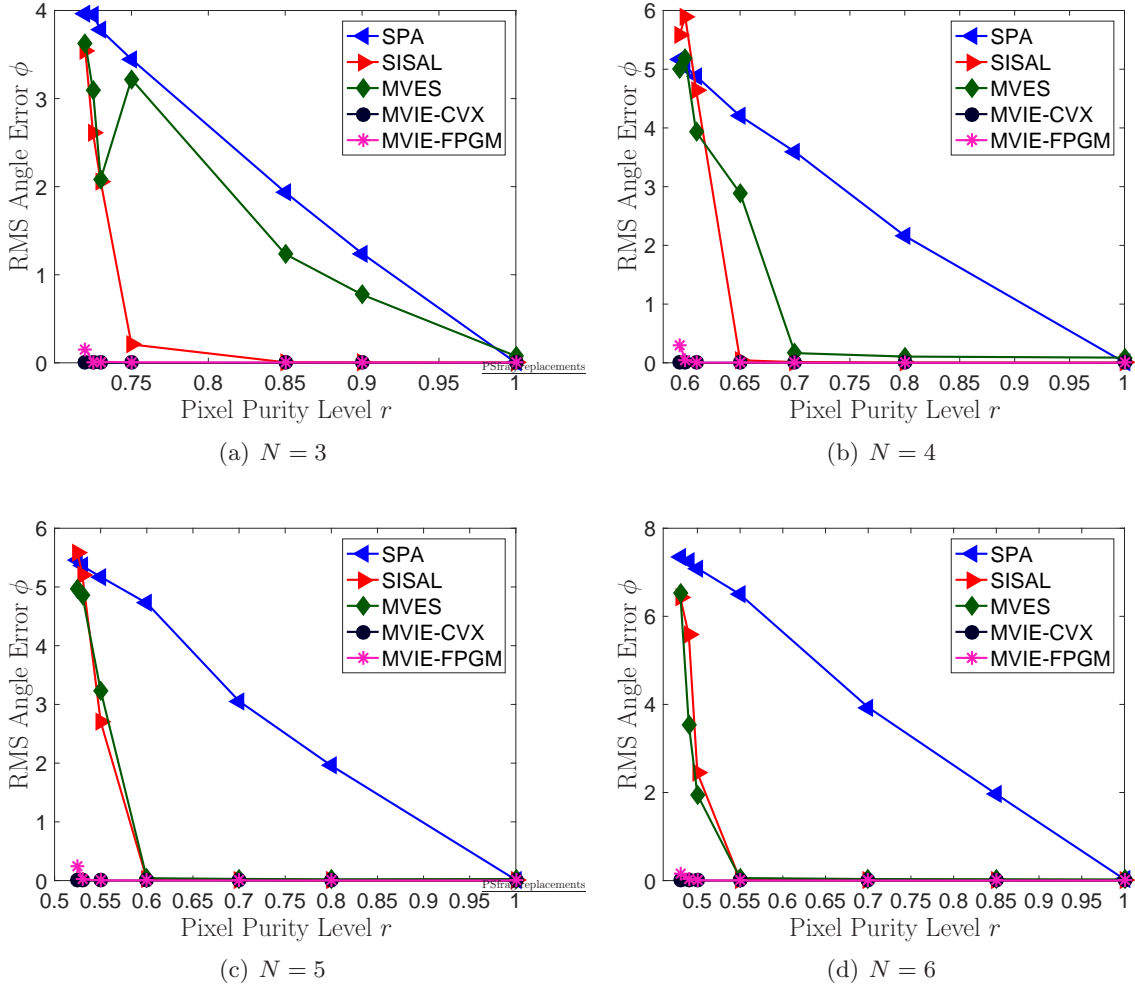


Figure 4: Recovery performance of the SSMF algorithms with respect to the numerically controlled pixel purity level r . $M = 224, L = 1,000$, the noiseless case.

the SNR is at 40dB. We see that SISAL may perform slightly better than MVIE when the pixel purity level r is not too small. However, we also see that for a range of small values of r , SISAL exhibits the same performance degradation issue as in the noiseless case.

It is also interesting to examine runtime performance of the various algorithms. The results are shown in Table 1. We see that MVIE-CVX is slow, and this is because of the runtimes required for the general-purpose convex optimization software CVX to process the MVIE problem. In comparison, MVIE-FPGM, which uses a custom-derived algorithm for the MVIE problem, runs much faster than MVIE-CVX. Also, MVIE-FPGM is faster than MVES but is slower than SISAL for $N \geq 5$.

In the previous section we discussed the computational bottleneck of MVIE arising from facet enumeration. To get some ideas, we show the detailed runtimes of MVIE-FPGM in Table 2. As can be seen, facet enumeration does not incur the majority of computations of the whole MVIE-FPGM

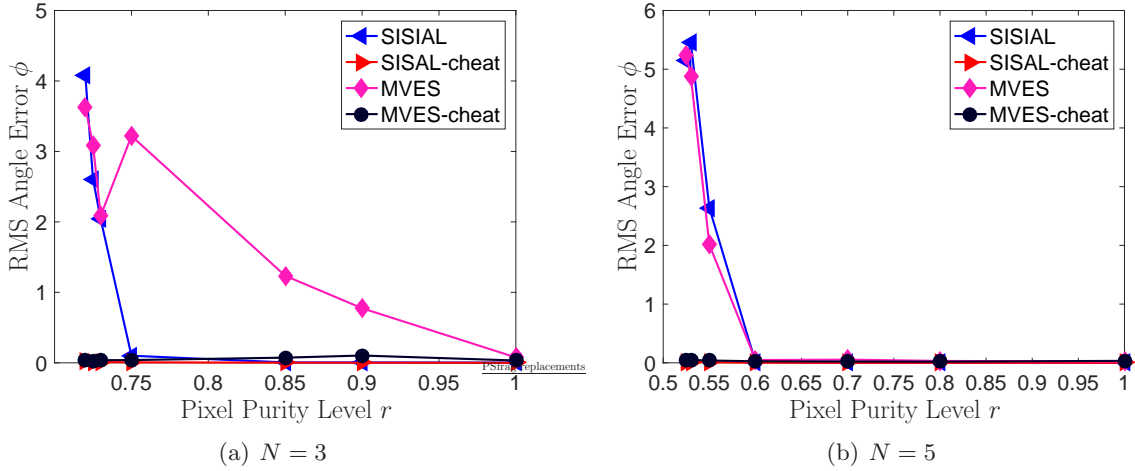


Figure 5: Recovery performance of MVES and SISAL under different initializations.

process. Instead, it is the process of solving the MVIE optimization problem that takes up the bulk of the total complexity. A reason for this is that facet enumeration may output a large number of halfspaces K , and consequently solving the MVIE problem becomes computationally harder. While we should recall that the main contribution of this paper is to introduce a new theoretical SSMF framework through MVIE, as a future direction it would be interesting to study how we can further improve algorithm designs through considering both facet enumeration and MVIE optimization.

7 Conclusion

In this paper we have established a new SSMF framework through analyzing an MVIE problem. As the main contribution, we showed that the MVIE framework can admit exact recovery beyond separable or pure-pixel problem instances, and that its exact recovery condition is as good as that of the MVES framework. However, unlike MVES which requires one to solve a non-convex problem, the MVIE framework suggests a two-step solution, namely, facet enumeration and convex optimization. The viability of the MVIE framework was verified by numerical results, and it was illustrated that MVIE exhibits stable performance over a wide range of pixel purity levels. We hope this new framework might inspire more theoretical and practical results in tackling SSMF.

A Proof of Proposition 1

We will use the following results.

Fact 3 *Let $f(\boldsymbol{\alpha}) = \boldsymbol{\Phi}\boldsymbol{\alpha} + \mathbf{b}$ where $(\boldsymbol{\Phi}, \mathbf{b}) \in \mathbb{R}^{m \times n} \times \mathbb{R}^m$ and $\boldsymbol{\Phi}$ has full column rank. The following results hold.*

(a) *Let \mathcal{C} be a non-empty set in \mathbb{R}^m with $\mathcal{C} \subseteq \mathcal{A}(\boldsymbol{\Phi}, \mathbf{b})$. Then*

$$\text{rbd}(f^{-1}(\mathcal{C})) = f^{-1}(\text{rbd } \mathcal{C}).$$

Table 1: Runtimes (sec.) of the various algorithms. The simulation settings are the same as those in Figure 4.

N	r	SPA	SISAL	MVES	MVIE-CVX	MVIE-FPGM
3	0.72	0.007	0.275	0.271	0.626	0.064
	0.85	0.007	0.271	0.727	0.468	0.060
	1	0.006	0.270	1.707	0.305	0.066
4	0.595	0.011	0.306	0.808	4.098	0.208
	0.8	0.009	0.299	3.603	2.647	0.064
	1	0.006	0.297	5.627	1.400	0.096
5	0.525	0.011	0.343	2.595	32.381	1.264
	0.8	0.012	0.342	10.334	20.458	0.974
	1	0.008	0.333	11.357	8.869	0.736
6	0.48	0.014	0.388	3.850	380.572	4.960
	0.7	0.013	0.388	19.822	543.374	6.456
	1	0.008	0.384	20.466	121.569	3.498

Table 2: Detailed runtimes (sec.) of MVIE-FPGM. The simulation settings are the same as those in Figure 4.

N	r	Total	Facet enumeration	FPGM + others
3	0.72	0.064	0.007	0.056
	0.85	0.060	0.007	0.053
	1	0.066	0.007	0.059
4	0.595	0.208	0.023	0.185
	0.8	0.064	0.017	0.047
	1	0.096	0.012	0.085
5	0.525	1.264	0.111	1.153
	0.8	0.974	0.092	0.882
	1	0.736	0.049	0.687
6	0.48	4.960	0.592	4.368
	0.7	6.456	0.797	5.659
	1	3.498	0.376	3.122

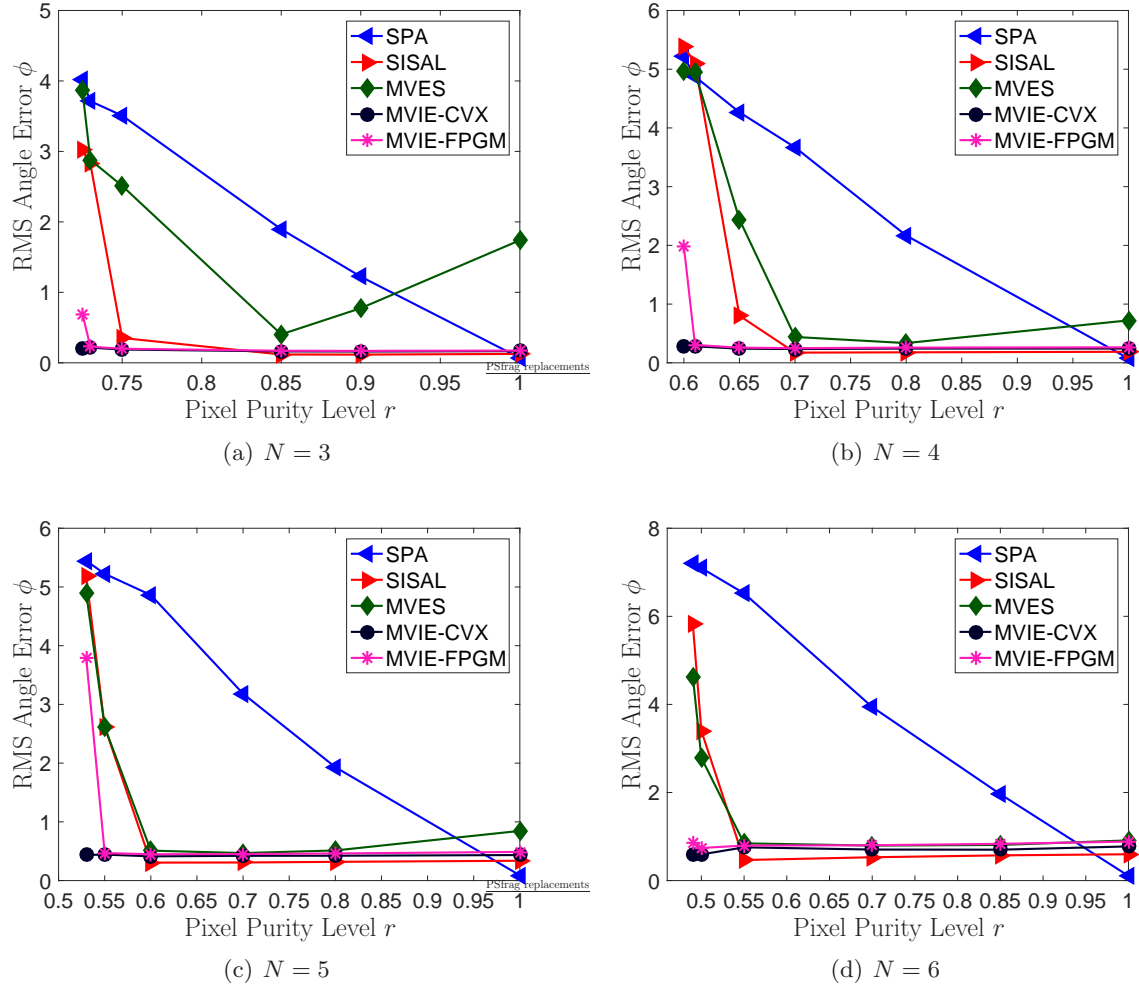


Figure 6: Recovery performance of the SSMF algorithms with respect to the numerically controlled pixel purity level r . $M = 224, L = 1,000$, SNR = 40dB.

(b) Let $\mathcal{C}_1, \mathcal{C}_2$ be sets in \mathbb{R}^m with $\mathcal{C}_1, \mathcal{C}_2 \subseteq \mathcal{A}(\Phi, \mathbf{b})$. Then

$$\mathcal{C}_1 \subseteq \mathcal{C}_2 \iff f^{-1}(\mathcal{C}_1) \subseteq f^{-1}(\mathcal{C}_2).$$

The results in the above fact may be easily deduced or found in textbooks.

First, we prove the feasibility results in Statements (a)–(b) of Proposition 1. Let (\mathbf{F}, \mathbf{c}) be a feasible solution to Problem (4). Since

$$\mathcal{E}(\mathbf{F}, \mathbf{c}) \subseteq \mathcal{X} \subseteq \text{aff}\{\mathbf{x}_1, \dots, \mathbf{x}_L\} = \mathcal{A}(\Phi, \mathbf{b}),$$

it holds that

$$\mathbf{f}_i + \mathbf{c} = \Phi \boldsymbol{\alpha}_i + \mathbf{b}, \quad i = 1, \dots, N, \quad \mathbf{c} = \Phi \mathbf{c}' + \mathbf{b},$$

for some $\boldsymbol{\alpha}_1, \dots, \boldsymbol{\alpha}_N, \mathbf{c}' \in \mathbb{R}^{N-1}$. By letting $\mathbf{f}'_i = \boldsymbol{\alpha}_i - \mathbf{c}', i = 1, \dots, N$, one can show that $\mathbf{F}' = [\mathbf{f}'_1, \dots, \mathbf{f}'_N]$ and \mathbf{c}' are uniquely given by $(\mathbf{F}', \mathbf{c}') = (\Phi^\dagger \mathbf{F}, \Phi^\dagger(\mathbf{c} - \mathbf{b}))$. Also, by letting $f(\boldsymbol{\alpha}) = \Phi\boldsymbol{\alpha} + \mathbf{b}$, it can be verified that

$$f^{-1}(\mathcal{E}(\mathbf{F}, \mathbf{c})) = \mathcal{E}(\mathbf{F}', \mathbf{c}').$$

Similarly, for \mathcal{X} , we have $\mathbf{x}_i \in \mathcal{X} \subseteq \mathcal{A}(\Phi, \mathbf{b})$. This means that \mathbf{x}_i can be expressed as $\mathbf{x}_i = \Phi\mathbf{x}'_i + \mathbf{b}$ for some $\mathbf{x}'_i \in \mathbb{R}^{N-1}$, and it can be verified that \mathbf{x}'_i is uniquely given by $\mathbf{x}'_i = \Phi^\dagger(\mathbf{x}_i - \mathbf{b})$. Subsequently it can be further verified that

$$f^{-1}(\mathcal{X}) = \mathcal{X}'.$$

Hence, by using Fact 3.(b) via setting $\mathcal{C}_1 = \mathcal{E}(\mathbf{F}, \mathbf{c})$, $\mathcal{C}_2 = \mathcal{X}$, we get $\mathcal{E}(\mathbf{F}', \mathbf{c}') \subseteq \mathcal{X}'$. Thus, $(\mathbf{F}', \mathbf{c}')$ is a feasible solution to Problem (9), and we have proven the feasibility result in Statement (a) of Proposition 1. The proof of the feasibility result in Statement (b) of Proposition 1 follows the same proof method, and we omit it for brevity.

Second, we prove the optimality results in Statements (a)–(b) of Proposition 1. Let (\mathbf{F}, \mathbf{c}) be an optimal solution to Problem (4), $(\mathbf{F}', \mathbf{c}')$ be equal to $(\Phi^\dagger \mathbf{F}, \Phi^\dagger(\mathbf{c} - \mathbf{b}))$ which is feasible to Problem (9), and v_{opt} be the optimal value of Problem (4). Then we have

$$v_{\text{opt}} = \det(\mathbf{F}^T \mathbf{F}) = \det((\mathbf{F}')^T \Phi^T \Phi \mathbf{F}) = |\det(\mathbf{F}')|^2 \det(\Phi^T \Phi) \geq v'_{\text{opt}} \det(\Phi^T \Phi),$$

where v'_{opt} denotes the optimal value of Problem (9). Conversely, by redefining $(\mathbf{F}', \mathbf{c}')$ as an optimal solution to Problem (9) and $(\mathbf{F}, \mathbf{c}) = (\Phi\mathbf{F}', \Phi\mathbf{c}' + \mathbf{b})$ (which is feasible to Problem (4)), we also get

$$v'_{\text{opt}} = |\det(\mathbf{F}')|^2 = \frac{1}{\det(\Phi^T \Phi)} \det(\mathbf{F}^T \mathbf{F}) \geq \frac{1}{\det(\Phi^T \Phi)} v_{\text{opt}}.$$

The above two equations imply $v_{\text{opt}} = v'_{\text{opt}} \det(\Phi^T \Phi)$, and it follows that the optimal solution results in Statements (a)–(b) of Proposition 1 are true.

Third, we prove Statement (c) of Proposition 1. Recall from (3) that $\dim \mathcal{X} = N - 1$ (also recall that the result is based on the premise of (A2)–(A3)). From the development above, one can show that

$$\mathcal{X} = \{\Phi\mathbf{x}' + \mathbf{b} \mid \mathbf{x}' \in \mathcal{X}'\}.$$

It can be further verified from the above equation and the full column rank property of Φ that $\dim \mathcal{X}' = \dim \mathcal{X} = N - 1$ must hold. In addition, as a basic convex analysis result, a convex set \mathcal{C} in \mathbb{R}^m has non-empty interior if $\dim \mathcal{C} = m$. This leads us to the conclusion that \mathcal{X}' has non-empty interior.

Finally, we prove Statement (d) of Proposition 1. The results therein are merely applications of Fact 3; e.g., $\mathcal{C}_1 = \{\mathbf{q}\}$, $\mathcal{C}_2 = \mathcal{E}$ for $\mathbf{q} \in \mathcal{E} \implies \mathbf{q}' \in \mathcal{E}'$, $\mathcal{C}_1 = \{\mathbf{q}\}$, $\mathcal{C}_2 = \text{rbd } \mathcal{X}$ for $\mathbf{q} \in \text{rbd } \mathcal{X} \implies \mathbf{q}' \in \text{rbd}(f^{-1}(\mathcal{X})) = \text{bd } \mathcal{X}'$, and so forth.

B Fast Proximal Gradient Algorithm for Handling Problem (32)

In this appendix we derive a fast algorithm for handling the MVIE problem in (32). Let us describe the formulation used. Instead of solving Problem (32) directly, we employ an approximate formulation as follows

$$\min_{\mathbf{F}' \in \mathbb{S}_+^{N-1}, \mathbf{c}' \in \mathbb{R}^{N-1}} -\log \det(\mathbf{F}') + \rho \sum_{i=1}^K \psi(\|\mathbf{F}' \mathbf{g}_i\| + \mathbf{g}_i^T \mathbf{c}' - h_i), \quad (34)$$

for a pre-specified constant $\rho > 0$ and for some convex differentiable function $\psi : \mathbb{R} \rightarrow \mathbb{R}$ such that $\psi(x) = 0$ for $x \leq 0$ and $\psi(x) > 0$ for $x > 0$; specifically our choice of ψ is the one-sided Huber function, i.e.,

$$\psi(z) = \begin{cases} 0, & z < 0, \\ \frac{1}{2}z^2, & 0 \leq z \leq 1, \\ z - \frac{1}{2}, & z > 1. \end{cases}$$

Our approach is to use a penalized, or “soft-constrained”, convex formulation in place of Problem (32), whose SOC constraints may not be easy to deal with in the “hard-constrained” sense. Problem (34) has a nondifferentiable and unbounded-above objective function. To facilitate our algorithm design efforts later, we further approximate the problem by

$$\min_{\mathbf{F}' \in \mathcal{W}, \mathbf{c}' \in \mathbb{R}^{N-1}} -\log \det(\mathbf{F}') + \rho \sum_{i=1}^K \psi(\sqrt{\|\mathbf{F}' \mathbf{g}_i\|^2 + \epsilon} + \mathbf{g}_i^T \mathbf{c}' - h_i), \quad (35)$$

for some small constant $\epsilon > 0$, where $\mathcal{W} \triangleq \{\mathbf{W} \in \mathbb{S}^{N-1} \mid \lambda_{\min}(\mathbf{W}) \geq \epsilon\}$.

Now we describe the algorithm. We employ the fast proximal gradient method (FPGM) or FISTA [6], which is known to guarantee a convergence rate of $\mathcal{O}(1/k^2)$ under certain premises; here, k is the iteration number. For notational convenience, let us denote $n = N - 1$, $\mathbf{W} = \mathbf{F}'$, $\mathbf{y} = \mathbf{c}'$, and rewrite Problem (35) as

$$\min_{\substack{\mathbf{W} \in \mathbb{R}^{n \times n} \\ \mathbf{y} \in \mathbb{R}^n}} \underbrace{\sum_{i=1}^K \psi\left(\sqrt{\|\mathbf{W} \mathbf{g}_i\|^2 + \epsilon} + \mathbf{g}_i^T \mathbf{y} - h_i\right)}_{\triangleq f(\mathbf{W}, \mathbf{y})} + \underbrace{I_{\mathcal{W}}(\mathbf{W}) - \frac{1}{\rho} \log \det(\mathbf{W})}_{\triangleq g(\mathbf{W})}, \quad (36)$$

where $I_{\mathcal{W}}(\cdot)$ is the indicator function of \mathcal{W} . By applying FPGM to the formulation in (36), we obtain Algorithm 2. In the algorithm, the notation $\langle \cdot, \cdot \rangle$ stands for the inner product, $\|\cdot\|$ still stands for the Euclidean norm, ψ' is the differentiation of ψ , and $\text{prox}_f(\mathbf{z}) = \arg \min_{\mathbf{x}} \frac{1}{2} \|\mathbf{z} - \mathbf{x}\|^2 + f(\mathbf{x})$ is the proximal mapping of f . The algorithm requires computations of the proximal mapping $\text{prox}_{tg}(\mathbf{W} - t \nabla_{\mathbf{W}} f)$. The solution to our proximal mapping is described in the following fact.

Fact 4 Consider the proximal mapping $\text{prox}_{tg}(\mathbf{V})$ where the function g has been defined in (36) and $t > 0$. Let $\mathbf{V}_{\text{sym}} = \frac{1}{2}(\mathbf{V} + \mathbf{V}^T)$, and let $\mathbf{V}_{\text{sym}} = \mathbf{U} \mathbf{\Lambda} \mathbf{U}^T$ be the symmetric eigendecomposition of \mathbf{V}_{sym} where $\mathbf{U} \in \mathbb{R}^{n \times n}$ is orthogonal and $\mathbf{\Lambda} \in \mathbb{R}^{n \times n}$ is diagonal with diagonal elements given by $\lambda_1, \dots, \lambda_n$. We have

$$\text{prox}_{tg}(\mathbf{V}) = \mathbf{U} \mathbf{D} \mathbf{U}^T$$

where $\mathbf{D} \in \mathbb{R}^{n \times n}$ is diagonal with diagonal elements given by $d_i = \max \left\{ \frac{\lambda_i + \sqrt{\lambda_i^2 + 4t/\rho}}{2}, \epsilon \right\}$, $i = 1, \dots, n$.

The proof of the above fact will be given in Appendix B.1. Furthermore, we should mention convergence. FPGM is known to have a $\mathcal{O}(1/k^2)$ convergence rate if the problem is convex and f has a Lipschitz continuous gradient. In Appendix B.2, we show that f has a Lipschitz continuous gradient.

Algorithm 2 FPGM for Solving Problem (36)

- 1: **Given** $\epsilon > 0$, $\rho > 0$, $(\mathbf{g}_i, h_i)_{i=1}^K$, $t_{\max} > 0$, $\beta \in (0, 1)$, and a starting point $(\mathbf{W}, \mathbf{y}) \in \mathcal{W} \times \mathbb{R}^n$.
- 2: Set $k := 1$, $u_0 = 0$, $(\mathbf{W}^0, \mathbf{y}^0) = (\mathbf{W}, \mathbf{y})$.
- 3: **repeat**
- 4: $\nabla_{\mathbf{W}} f := \sum_{i=1}^K \frac{\psi'(\sqrt{\|\mathbf{W}\mathbf{g}_i\|^2 + \epsilon} + \mathbf{g}_i^T \mathbf{y} - h_i)}{\sqrt{\|\mathbf{W}\mathbf{g}_i\|^2 + \epsilon}} (\mathbf{W}\mathbf{g}_i\mathbf{g}_i^T)$;
- 5: $\nabla_{\mathbf{y}} f := \sum_{i=1}^K \psi'(\sqrt{\|\mathbf{W}\mathbf{g}_i\|^2 + \epsilon} + \mathbf{g}_i^T \mathbf{y} - h_i) \mathbf{g}_i$;
- 6: $t := t_{\max}$;
- 7: $\mathbf{W}^k := \text{prox}_{tg}(\mathbf{W} - t\nabla_{\mathbf{W}} f)$, $\mathbf{y}^k := \mathbf{y} - t\nabla_{\mathbf{y}} f$;
- 8: % line search
- 9: **while** $f(\mathbf{W}^k, \mathbf{y}^k) > f(\mathbf{W}, \mathbf{y}) + \langle (\nabla_{\mathbf{W}} f, \nabla_{\mathbf{y}} f), (\mathbf{W}^k, \mathbf{y}^k) - (\mathbf{W}, \mathbf{y}) \rangle + \frac{1}{2t} \|(\mathbf{W}^k, \mathbf{y}^k) - (\mathbf{W}, \mathbf{y})\|^2$ **do**
- 10: $t := \beta t$;
- 11: $\mathbf{W}^k := \text{prox}_{tg}(\mathbf{W} - t\nabla_{\mathbf{W}} f)$, $\mathbf{y}^k := \mathbf{y} - t\nabla_{\mathbf{y}} f$;
- 12: **end while**
- 13: $u_k = \frac{1}{2} \left(1 + \sqrt{1 + 4u_{k-1}^2} \right)$;
- 14: $(\mathbf{W}, \mathbf{y}) := (\mathbf{W}^k, \mathbf{y}^k) + \frac{u_{k-1}-1}{u_k} ((\mathbf{W}^k, \mathbf{y}^k) - (\mathbf{W}^{k-1}, \mathbf{y}^{k-1}))$;
- 15: $k := k + 1$;
- 16: **until** a pre-specified stopping rule is satisfied.
- 17: **Output** $(\mathbf{W}^{k-1}, \mathbf{y}^{k-1})$.

B.1 Proof of Fact 4

It can be verified that for any symmetric \mathbf{W} , we have $\|\mathbf{V} - \mathbf{W}\|^2 = \|\mathbf{V}_{\text{sym}} - \mathbf{W}\|^2 + \|\frac{1}{2}(\mathbf{V} - \mathbf{V}^T)\|^2$. Thus, the proximal mapping $\text{prox}_{tg}(\mathbf{V})$ can be written as

$$\text{prox}_{tg}(\mathbf{V}) = \arg \min_{\mathbf{W} \in \mathcal{W}} \frac{1}{2} \|\mathbf{V}_{\text{sym}} - \mathbf{W}\|^2 - \frac{t}{\rho} \log \det(\mathbf{W}) \quad (37)$$

Let $\mathbf{V}_{\text{sym}} = \mathbf{U}\mathbf{\Lambda}\mathbf{U}^T$ be the symmetric eigendecomposition of \mathbf{V}_{sym} . Also, let $\tilde{\mathbf{W}} = \mathbf{U}^T \mathbf{W} \mathbf{U}$, and note that $\mathbf{W} \in \mathcal{W}$ implies $\tilde{\mathbf{W}} \in \mathcal{W}$. We have the following inequality for any $\mathbf{W} \in \mathcal{W}$:

$$\begin{aligned} \frac{1}{2} \|\mathbf{V}_{\text{sym}} - \mathbf{W}\|^2 - \frac{t}{\rho} \log \det(\mathbf{W}) &= \frac{1}{2} \|\mathbf{\Lambda} - \tilde{\mathbf{W}}\|^2 - \frac{t}{\rho} \log \det(\tilde{\mathbf{W}}) \\ &\geq \sum_{i=1}^n \frac{1}{2} (\lambda_i - \tilde{w}_{ii})^2 - \frac{t}{\rho} \log(\tilde{w}_{ii}) \\ &\geq \sum_{i=1}^n \min_{\tilde{w}_{ii} \geq \epsilon} \left[\frac{1}{2} (\lambda_i - \tilde{w}_{ii})^2 - \frac{t}{\rho} \log(\tilde{w}_{ii}) \right] \end{aligned} \quad (38)$$

where the first equality is due to rotational invariance of the Euclidean norm and determinant; the second inequality is due to $\|\mathbf{\Lambda} - \tilde{\mathbf{W}}\|^2 \geq \sum_{i=1}^n (\lambda_i - \tilde{w}_{ii})^2$ and the Hadamard inequality $\det(\tilde{\mathbf{W}}) \leq \prod_{i=1}^n \tilde{w}_{ii}$; the third inequality is due to the fact that $\lambda_{\min}(\tilde{\mathbf{W}}) \leq \tilde{w}_{ii}$ for all i . One can readily show that the optimal solution to the problem in (38) is $\tilde{w}_{ii}^* = \max \left\{ \left(\lambda_i + \sqrt{\lambda_i^2 + 4t/\rho} \right) / 2, \epsilon \right\}$. Furthermore, by letting $\mathbf{W}^* = \mathbf{U}\mathbf{D}\mathbf{U}^T$, $\mathbf{D} = \text{Diag}(\tilde{w}_{11}^*, \dots, \tilde{w}_{nn}^*)$, the equalities in (38) are attained. Since \mathbf{W}^* also lies in \mathcal{W} , we conclude that \mathbf{W}^* is the optimal solution to the problem in (37).

B.2 Lipschitz Continuous Gradient Property of f

In this appendix we show that the function f in (36) has a Lipschitz constant gradient. To this end, define $\mathbf{z} = [(\text{vec}(\mathbf{W}))^T, \mathbf{y}^T]^T$ and

$$\phi_i(\mathbf{z}) = \sqrt{\|\mathbf{C}_i \mathbf{z}\|^2 + \epsilon} + \mathbf{d}_i^T \mathbf{z} - h_i, \quad i = 1, \dots, K,$$

where $\mathbf{C}_i = [(\mathbf{g}_i^T \otimes \mathbf{I}), \mathbf{0}]$ (here “ \otimes ” denotes the Kronecker product) and $\mathbf{d}_i = [\mathbf{0}^T, \mathbf{g}_i^T]^T$. Then, f can be written as $f(\mathbf{W}, \mathbf{y}) = \sum_{i=1}^K \psi(\phi_i(\mathbf{z}))$. From the above equation, we see that f has a Lipschitz continuous gradient if every $\psi(\phi_i(\mathbf{z}))$ has a Lipschitz continuous gradient. Hence, we seek to prove the latter. Consider the following fact.

Fact 5 *Let $\psi : \mathbb{R} \rightarrow \mathbb{R}$, $\phi : \mathbb{R}^n \rightarrow \mathbb{R}$ be functions that satisfy the following properties:*

- (a) ψ' is bounded on \mathbb{R} and ψ has a Lipschitz continuous gradient on \mathbb{R} ;
- (b) $\nabla \phi$ is bounded on \mathbb{R}^n and ϕ has a Lipschitz continuous gradient on \mathbb{R}^n .

Then, $\psi(\phi(\mathbf{z}))$ has a Lipschitz continuous gradient on \mathbb{R}^n .

As Fact 5 can be easily proved from the definition of Lipschitz continuity, its proof is omitted here for conciseness. Recall that for our problem, ψ is the one-sided Huber function. One can verify that the one-sided Huber function has bounded ψ' and Lipschitz continuous gradient. As for ϕ_i , let us first evaluate its gradient and Hessian

$$\begin{aligned} \nabla \phi_i(\mathbf{z}) &= \frac{\mathbf{C}_i^T \mathbf{C}_i \mathbf{z}}{\sqrt{\|\mathbf{C}_i \mathbf{z}\|^2 + \epsilon}} + \mathbf{d}_i, \\ \nabla^2 \phi_i(\mathbf{z}) &= \frac{\mathbf{C}_i^T \mathbf{C}_i}{\sqrt{\|\mathbf{C}_i \mathbf{z}\|^2 + \epsilon}} - \frac{(\mathbf{C}_i^T \mathbf{C}_i \mathbf{z})(\mathbf{C}_i^T \mathbf{C}_i \mathbf{z})^T}{(\|\mathbf{C}_i \mathbf{z}\|^2 + \epsilon)^{3/2}}. \end{aligned}$$

We have

$$\|\nabla \phi_i(\mathbf{z})\| \leq \|\mathbf{d}_i\| + \frac{\|\mathbf{C}_i^T \mathbf{C}_i \mathbf{z}\|}{\sqrt{\|\mathbf{C}_i \mathbf{z}\|^2 + \epsilon}} \leq \|\mathbf{d}_i\| + \frac{\sigma_{\max}(\mathbf{C}_i) \|\mathbf{C}_i \mathbf{z}\|}{\sqrt{\|\mathbf{C}_i \mathbf{z}\|^2 + \epsilon}} \leq \|\mathbf{d}_i\| + \sigma_{\max}(\mathbf{C}_i),$$

where $\sigma_{\max}(\mathbf{X})$ denotes the largest singular value of \mathbf{X} . Hence, $\nabla \phi_i(\mathbf{z})$ is bounded. Moreover, recall that a function has a Lipschitz continuous gradient if its Hessian is bounded. Since

$$\|\nabla^2 \phi_i(\mathbf{z})\| \leq \sqrt{n + n^2} \lambda_{\max}(\nabla^2 \phi_i(\mathbf{z})) \leq \sqrt{n + n^2} \lambda_{\max} \left(\frac{\mathbf{C}_i^T \mathbf{C}_i}{\sqrt{\|\mathbf{C}_i \mathbf{z}\|^2 + \epsilon}} \right) \leq \frac{\sqrt{n + n^2} \lambda_{\max}(\mathbf{C}_i^T \mathbf{C}_i)}{\sqrt{\epsilon}},$$

the function ϕ_i has a Lipschitz continuous gradient. The desired result is therefore proven.

References

[1] S. ARORA, R. GE, Y. HALPERN, D. MIMNO, A. MOITRA, D. SONTAG, Y. WU, AND M. ZHU, *A practical algorithm for topic modeling with provable guarantees*, in International Conference on Machine Learning, 2013, pp. 280–288.

[2] S. ARORA, R. GE, R. KANNAN, AND A. MOITRA, *Computing a nonnegative matrix factorization—Provably*, in Proceedings of the forty-fourth annual ACM symposium on Theory of computing, ACM, 2012, pp. 145–162.

[3] D. AVIS, D. BREMNER, AND R. SEIDEL, *How good are convex hull algorithms?*, Computational Geometry, 7 (1997), pp. 265–301.

[4] C. B. BARBER, D. P. DOBKIN, AND H. HUHDANPAA, *The quickhull algorithm for convex hulls*, ACM Transactions on Mathematical Software (TOMS), 22 (1996), pp. 469–483.

[5] S. BAROT AND J. A. TAYLOR, *A concise, approximate representation of a collection of loads described by polytopes*, International Journal of Electrical Power & Energy Systems, 84 (2017), pp. 55–63.

[6] A. BECK AND M. TEBoulle, *A fast iterative shrinkage-thresholding algorithm for linear inverse problems*, SIAM journal on imaging sciences, 2 (2009), pp. 183–202.

[7] J. BLOUCAS-DIAS, *A variable splitting augmented Lagrangian approach to linear spectral unmixing*, in Proc. IEEE WHISPERS, Aug. 2009.

[8] J. BLOUCAS-DIAS, A. PLAZA, N. DOBIGEON, M. PARENTE, Q. DU, P. GADER, AND J. CHANUSSOT, *Hyperspectral unmixing overview: Geometrical, statistical, and sparse regression-based approaches*, IEEE J. Sel. Topics Appl. Earth Observ., 5 (2012), pp. 354–379.

[9] J. W. BOARDMAN, F. A. KRUSE, AND R. O. GREEN, *Mapping target signatures via partial unmixing of AVIRIS data*, in The Fifth Annual JPL Airborne Earth Science Workshop, 1995, pp. 23–26.

[10] E. BOROS, K. ELBASSIONI, V. GURVICH, AND K. MAKINO, *Generating vertices of polyhedra and related problems of monotone generation*, Centre de Recherches Mathématiques (CRM), 49 (2009), pp. 15–43.

[11] S. BOYD AND L. VANDENBERGHE, *Convex Optimization*, Cambridge University Press, 2004.

[12] D. BREMNER, K. FUKUDA, AND A. MARZETTA, *Primal-dual methods for vertex and facet enumeration*, Discrete & Computational Geometry, 20 (1998), pp. 333–357.

[13] D. D. BREMNER, *On the complexity of vertex and facet enumeration for convex polytopes*, PhD thesis, Citeseer, 1997.

[14] T.-H. CHAN, C.-Y. CHI, Y.-M. HUANG, AND W.-K. MA, *A convex analysis based minimum-volume enclosing simplex algorithm for hyperspectral unmixing*, IEEE Trans. Signal Process., 57 (2009), pp. 4418–4432.

[15] T.-H. CHAN, W.-K. MA, A. AMBIKAPATHI, AND C.-Y. CHI, *A simplex volume maximization framework for hyperspectral endmember extraction*, IEEE Trans. Geosci. Remote Sens., 49 (2011), pp. 4177–4193.

[16] T.-H. CHAN, W.-K. MA, C.-Y. CHI, AND Y. WANG, *A convex analysis framework for blind separation of non-negative sources*, IEEE Transactions on Signal Processing, 56 (2008), pp. 5120–5134.

[17] L. CHEN, P. L. CHOYKE, T.-H. CHAN, C.-Y. CHI, G. WANG, AND Y. WANG, *Tissue-specific compartmental analysis for dynamic contrast-enhanced MR imaging of complex tumors*, IEEE Trans. Medical Imaging, 30 (2011), pp. 2044–2058.

[18] R. CLARK, G. SWAYZE, R. WISE, E. LIVO, T. HOEFEN, R. KOKALY, AND S. SUTLEY, *USGS digital spectral library splib06a: U.S. Geological Survey, Digital Data Series 231*. <http://speclab.cr.usgs.gov/spectral.lib06>, 2007.

[19] T. H. CORMEN, C. E. LEISERSON, R. L. RIVEST, AND C. STEIN, *Introduction to Algorithms*, The MIT Press (2nd Edition), 2001.

[20] M. D. CRAIG, *Minimum-volume transforms for remotely sensed data*, IEEE Trans. Geosci. Remote Sens., 32 (1994), pp. 542–552.

[21] E. ELHAMIFAR, G. SAPIRO, AND R. VIDAL, *See all by looking at a few: Sparse modeling for finding representative objects*, in IEEE Computer Vision and Pattern Recognition (CVPR), 2012, pp. 1600–1607.

[22] E. ESSER, M. MOLLER, S. OSHER, G. SAPIRO, AND J. XIN, *A convex model for nonnegative matrix factorization and dimensionality reduction on physical space*, IEEE Transactions on Image Processing, 21 (2012), pp. 3239–3252.

[23] X. FU, K. HUANG, B. YANG, W.-K. MA, AND N. D. SIDIROPOULOS, *Robust volume minimization-based matrix factorization for remote sensing and document clustering*, IEEE Transactions on Signal Processing, 64 (2016), pp. 6254–6268.

[24] X. FU AND W.-K. MA, *Robustness analysis of structured matrix factorization via self-dictionary mixed-norm optimization*, IEEE Signal Processing Letters, 23 (2016), pp. 60–64.

[25] X. FU, W.-K. MA, T.-H. CHAN, AND J. M. BIOCAS-DIAS, *Self-dictionary sparse regression for hyperspectral unmixing: Greedy pursuit and pure pixel search are related*, IEEE Journal of Selected Topics in Signal Processing, 9 (2015), pp. 1128–1141.

[26] X. FU, W.-K. MA, K. HUANG, AND N. D. SIDIROPOULOS, *Blind separation of quasi-stationary sources: Exploiting convex geometry in covariance domain*, IEEE Trans. Signal Processing, 63 (2015), pp. 2306–2320.

[27] W. E. FULL, R. EHRLICH, AND J. E. KLOVAN, *EXTENDED QMODEL—objective definition of external endmembers in the analysis of mixtures*, Mathematical Geology, 13 (1981), pp. 331–344.

[28] N. GILLIS, *Robustness analysis of hottopixx, a linear programming model for factoring nonnegative matrices*, SIAM Journal on Matrix Analysis and Applications, 34 (2013), pp. 1189–1212.

[29] N. GILLIS, *The why and how of nonnegative matrix factorization*, in Regularization, Optimization, Kernels, and Support Vector Machines, Chapman and Hall/CRC, 2014, pp. 257–291.

[30] N. GILLIS AND S. A. VAVASIS, *Fast and robust recursive algorithms for separable nonnegative matrix factorization*, IEEE Transactions on Pattern Analysis and Machine Intelligence, 36 (2014), pp. 698–714.

- [31] M. GRANT, S. BOYD, AND Y. YE, *CVX: Matlab software for disciplined convex programming*, 2008.
- [32] P. M. GRUBER AND F. E. SCHUSTER, *An arithmetic proof of John's ellipsoid theorem*, Archiv der Mathematik, 85 (2005), pp. 82–88.
- [33] K. HUANG, X. FU, AND N. D. SIDIROPOULOS, *Anchor-free correlated topic modeling: Identifiability and algorithm*, in Advances in Neural Information Processing Systems, 2016, pp. 1786–1794.
- [34] W. R. JOHNSON, D. W. WILSON, W. FINK, M. HUMAYUN, AND G. BEARMAN, *Snapshot hyperspectral imaging in ophthalmology*, Journal of biomedical optics, 12 (2007), pp. 014036–014036.
- [35] V. KLEE AND G. J. MINTY, *How good is the simplex algorithm?*, tech. report, DTIC Document, 1970.
- [36] J. LI AND J. BIOCAS-DIAS, *Minimum volume simplex analysis: A fast algorithm to unmix hyperspectral data*, in Proc. IEEE IGARSS, Aug. 2008.
- [37] C.-H. LIN, C.-Y. CHI, Y.-H. WANG, AND T.-H. CHAN, *A fast hyperplane-based minimum-volume enclosing simplex algorithm for blind hyperspectral unmixing*, IEEE Trans. Signal Process., 64 (Apr. 2016), pp. 1946–1961.
- [38] C.-H. LIN, W.-K. MA, W.-C. LI, C.-Y. CHI, AND A. AMBIKAPATHI, *Identifiability of the simplex volume minimization criterion for blind hyperspectral unmixing: The no-pure-pixel case*, IEEE Trans. Geosci. Remote Sens., 53 (2015), pp. 5530–5546.
- [39] M. B. LOPES, J. C. WOLFF, J. BIOCAS-DIAS, AND M. FIGUEIREDO, *NIR hyperspectral unmixing based on a minimum volume criterion for fast and accurate chemical characterisation of counterfeit tablets*, Analytical Chemistry, 82 (2010), pp. 1462–1469.
- [40] W.-K. MA, J. M. BIOCAS-DIAS, T.-H. CHAN, N. GILLIS, P. GADER, A. J. PLAZA, A. AMBIKAPATHI, AND C.-Y. CHI, *A signal processing perspective on hyperspectral unmixing*, IEEE Signal Process. Mag., 31 (2014), pp. 67–81.
- [41] W.-K. MA, T.-H. CHAN, C.-Y. CHI, AND Y. WANG, *Convex analysis for non-negative blind source separation with application in imaging*, in Convex Optimization in Signal Processing and Communications, D. P. Palomar and Y. C. Eldar, eds., Cambridge, UK: Cambridge Univ. Press, 2010.
- [42] J. M. NASCIMENTO AND J. M. DIAS, *Vertex component analysis: A fast algorithm to unmix hyperspectral data*, IEEE transactions on Geoscience and Remote Sensing, 43 (2005), pp. 898–910.
- [43] A. PACKER, *NP-hardness of largest contained and smallest containing simplices for V- and H-polytopes*, Discrete and Computational Geometry, 28 (2002), pp. 349–377.
- [44] B. RECHT, C. RE, J. TROPP, AND V. BITTORF, *Factoring nonnegative matrices with linear programs*, in Advances in Neural Information Processing Systems, 2012, pp. 1214–1222.

[45] N. WANG, E. P. HOFFMAN, L. CHEN, L. CHEN, Z. ZHANG, C. LIU, G. YU, D. M. HERRINGTON, R. CLARKE, AND Y. WANG, *Mathematical modelling of transcriptional heterogeneity identifies novel markers and subpopulations in complex tissues*, *Scientific reports*, 6 (2016), p. 18909.